

NASA/TP—2008–215473



Using the Inflection Points and Rates of Growth and Decay to Predict Levels of Solar Activity

Robert M. Wilson and David H. Hathaway
Marshall Space Flight Center, Marshall Space Flight Center, Alabama

The NASA STI Program...in Profile

Since its founding, NASA has been dedicated to the advancement of aeronautics and space science. The NASA Scientific and Technical Information (STI) Program Office plays a key part in helping NASA maintain this important role.

The NASA STI program operates under the auspices of the Agency Chief Information Officer. It collects, organizes, provides for archiving, and disseminates NASA's STI. The NASA STI program provides access to the NASA Aeronautics and Space Database and its public interface, the NASA Technical Report Server, thus providing one of the largest collections of aeronautical and space science STI in the world. Results are published in both non-NASA channels and by NASA in the NASA STI Report Series, which includes the following report types:

- **TECHNICAL PUBLICATION.** Reports of completed research or a major significant phase of research that present the results of NASA programs and include extensive data or theoretical analysis. Includes compilations of significant scientific and technical data and information deemed to be of continuing reference value. NASA's counterpart of peer-reviewed formal professional papers but has less stringent limitations on manuscript length and extent of graphic presentations.
- **TECHNICAL MEMORANDUM.** Scientific and technical findings that are preliminary or of specialized interest, e.g., quick release reports, working papers, and bibliographies that contain minimal annotation. Does not contain extensive analysis.
- **CONTRACTOR REPORT.** Scientific and technical findings by NASA-sponsored contractors and grantees.

- **CONFERENCE PUBLICATION.** Collected papers from scientific and technical conferences, symposia, seminars, or other meetings sponsored or cosponsored by NASA.
- **SPECIAL PUBLICATION.** Scientific, technical, or historical information from NASA programs, projects, and missions, often concerned with subjects having substantial public interest.
- **TECHNICAL TRANSLATION.** English-language translations of foreign scientific and technical material pertinent to NASA's mission.

Specialized services also include creating custom thesauri, building customized databases, and organizing and publishing research results.

For more information about the NASA STI program, see the following:

- Access the NASA STI program home page at <<http://www.sti.nasa.gov>>
- E-mail your question via the Internet to <help@sti.nasa.gov>
- Fax your question to the NASA STI Help Desk at 301-621-0134
- Phone the NASA STI Help Desk at 301-621-0390
- Write to:
NASA STI Help Desk
NASA Center for AeroSpace Information
7115 Standard Drive
Hanover, MD 21076-1320



Using the Inflection Points and Rates of Growth and Decay to Predict Levels of Solar Activity

Robert M. Wilson and David H. Hathaway

Marshall Space Flight Center, Marshall Space Flight Center, Alabama

National Aeronautics and
Space Administration

Marshall Space Flight Center • MSFC, Alabama 35812

Available from:

NASA Center for AeroSpace Information
7115 Standard Drive
Hanover, MD 21076-1320
301-621-0390

This report is also available in electronic form at
<https://www2.sti.nasa.gov>

TABLE OF CONTENTS

1. INTRODUCTION	1
2. RESULTS AND DISCUSSION	3
2.1 An Overview of Cyclic Behavior (Cycles 12–23)	3
2.2 Correlative Results	11
3. SUMMARY	34
REFERENCES	36

LIST OF FIGURES

1.	Variation of R for elapsed time in months $t=0$ –132 mo from $E(Rm)$	4
2.	Variation of ΔR for elapsed time in months $t=0$ –132 mo from $E(Rm)$	6
3.	Variation of 12-mma of ΔR for elapsed time in months $t=0$ –126 mo from $E(Rm)$...	7
4.	Variation of parametric values over cycles 12–23	8
5.	Variation of specific timing signatures based on ΔR	9
6.	Variation of specific timing signatures based on 12-mma of ΔR	10
7.	Scatter plot of RM versus $\Delta R_{\max pos}$	13
8.	Scatter plot of RM versus slope at $E(\Delta R_{\max pos})$	14
9.	Variation of $r^2(\Delta R(t))$	16
10.	Scatter plots of RM versus $\Delta R(t=10)$ and RM versus $\Delta R(t=25)$	17
11.	Scatter plot of RM versus (12-mma of ΔR) $\max pos$	18
12.	Variation of $r^2(12\text{-mma of } \Delta R(t))$	19
13.	Scatter plots of RM versus 12-mma of $\Delta R(t=8)$ and RM versus 12-mma of $\Delta R(t=22)$	20
14.	Scatter plot of PER versus $\Delta R_{\max neg}$	21
15.	Scatter plot of Rm (cycle $n+1$) versus $\Delta R_{\max neg}$	22
16.	Scatter plot of RM (cycle $n+1$) versus $\Delta R_{\max neg}$	23
17.	Scatter plot of PER versus (12-mma of ΔR) $\max neg$	24
18.	Scatter plot of Rm (cycle $n+1$) versus (12-mma of ΔR) $\max neg$	25
19.	Scatter plot of RM (cycle $n+1$) versus (12-mma of ΔR) $\max neg$	26
20.	Scatter plots of PER versus $\Delta R(T=30)$ and 12-mma of $\Delta R(T=31)$	27

21.	Scatter plots of Rm (cycle $n+1$) versus $\Delta R(T=31)$ and 12-mma of $\Delta R(T=27)$	28
22.	Scatter plots of RM (cycle $n+1$) versus $\Delta R(T=14)$ and 12-mma of $\Delta R(T=44)$	29
23.	Scatter plots of $Slope_{ASC}$ versus ΔR_{maxpos} and (12-mma of ΔR) $_{maxpos}$ and of $Slope_{DES}$ versus ΔR_{maxpos} and (12-mma of ΔR) $_{maxpos}$	31
24.	Scatter plots of $Slope_{DES}$ versus ΔR_{maxpos} , (12-mma of ΔR) $_{maxpos}$, and $Slope_{ASC}$	32
25.	Variation of cycle 23's R and 12-mma of ΔR for $t=0\text{--}135$ (May 1996–August 2007)	33

LIST OF TABLES

1.	Average parametric values for selected groupings of cycles	5
2.	Selected parametric values for sunspot cycles 12–23	11
3.	Correlations against sunspot cycle number	12

LIST OF ACRONYMS

12-mma	12-mo moving average
NOAA	National Oceanic and Atmospheric Administration

NOMENCLATURE

a	y -intercept in the regression equation
ASC	ascent duration (elapsed time from $E(Rm)$ to $E(RM)$)
$\langle ASC \rangle$	mean ascent duration
b	slope in the regression equation
cl	confidence level
DES	descent duration (elapsed time from $E(RM)$ to $E(Rm)$ of the following cycle)
$E(Rm)$	epoch of Rm
$E(RM)$	epoch of RM
$E(\Delta R_{\max neg})$	epoch of $\Delta R_{\max neg}$
$E(\Delta R_{\max pos})$	epoch of $\Delta R_{\max pos}$
P	probability
PER	period (cycle duration)
$\langle PER \rangle$	mean cycle period
r	coefficient of linear correlation
r^2	coefficient of determination
R	smoothed monthly mean sunspot number
Rm	sunspot minimum amplitude
$\langle Rm \rangle$	mean Rm
RM	sunspot maximum amplitude
$\langle RM \rangle$	mean RM

NOMENCLATURE (Continued)

ΔR	month-to-month change in R
ΔR_{maxneg}	maximum negative rate of change in R
ΔR_{maxpos}	maximum positive rate of change in R
sd	standard deviation
se	standard error of estimate
t	elapsed time in months from $E(R_m)$
$t(1)$	elapsed time in months from $E(R_m)$ to $E(\Delta R_{\text{maxpos}})$ or $E((12\text{-mma of } R)_{\text{maxpos}})$
$t(2)$	elapsed time in months from $E(\Delta R_{\text{maxpos}})$ or $E((12\text{-mma of } R)_{\text{maxpos}})$ to $E(RM)$
$t(3)$	elapsed time in months from $E(RM)$ to $E(\Delta R_{\text{maxneg}})$ or $E((12\text{-mma of } R)_{\text{maxneg}})$
$t(4)$	elapsed time in months from $E(\Delta R_{\text{maxneg}})$ or $E((12\text{-mma of } R)_{\text{maxneg}})$ to $E(R_m)$ of the following cycle
T	elapsed time in months from $E(RM)$
x	independent variable in the regression equation
y	dependent variable in the regression equation

TECHNICAL PUBLICATION

USING THE INFLECTION POINTS AND RATES OF GROWTH AND DECAY TO PREDICT LEVELS OF SOLAR ACTIVITY

1. INTRODUCTION

Sunspot cycles are conventionally described using 12-mo moving averages (12-mm_{as}) of monthly mean sunspot number, where (since 1981) the official number is now determined by the Sunspot Index Data Center <<http://sidc.oma.be/index.php3>>¹, located at the Royal Observatory of Belgium (in Brussels). Formerly, it was maintained at the Swiss Federal Observatory in Zurich, Switzerland. The minimum value of the 12-mm_a of monthly mean sunspot number is called the sunspot minimum amplitude (*Rm*) and its occurrence denotes the epoch of *Rm* (*E(Rm)*). Likewise, the maximum value of the 12-mm_a of monthly mean sunspot number is called sunspot maximum amplitude (*RM*) and its occurrence denotes the epoch of *RM* (*E(RM)*). In reality, sunspot minimum and maximum are better pictured as being broad intervals of time of several years in length when sunspot numbers are predominantly lower and higher, respectively, rather than being specific instances in time. While this is true, it is convenient to use the minimum and maximum values and their epochs of occurrence to describe the general characteristics of a sunspot cycle, such as its relative size, ascent duration (*ASC*), descent duration (*DES*), and cycle length (called period (*PER*)).

Following *Rm*, the sunspot number gradually increases in value, typically reaching a maximum rate of growth about 1–2 yr after *E(Rm)* and attaining *RM* about 3–5 yr after *E(Rm)*. The point of maximum positive rate of growth in sunspot number represents the ascending inflection point, and its numerical value has proven to be useful for estimating the later occurring *RM*.^{2–10} Likewise, during the declining portion of the sunspot cycle, there is a second inflection point (the descending inflection point), occurring typically about 6–7 yr after *Rm*, which seems to be related to the period of the ongoing sunspot cycle.²

The purpose of this Technical Publication is to reexamine the role of the inflection points and rates of growth and decay in sunspot cycle prediction on the basis of the behaviors of cycles 12–23, the most reliably determined sunspot cycles.^{11–13}

2. RESULTS AND DISCUSSION

2.1 An Overview of Cyclic Behavior (Cycles 12–23)

Figure 1 displays the mean cycle curve, based on epoch analysis and cycles 12–23 (the smoothed thick line) for elapsed time in months (t) from $E(Rm)$, $t=0$ –132 mo. The thin lines plotted above and below the mean cycle curve represent the upper and lower 90-percent prediction limits about each monthly value, respectively. The occurrence dates of $E(RM)$ relative to $E(Rm)$, which determines the ASC for each of the cycles, are noted across the top, and the actual RM values for the cycles are noted to the right. The respective PER for each of the cycles is noted near the bottom right, where cycle 23's PER is not shown since it remains ongoing. It should be noted, however, that the National Oceanic and Atmospheric Administration (NOAA) Solar Cycle 24 Prediction Panel¹⁴ has predicted cycle 24's official onset to occur about March 2008 \pm 6 mo, inferring that cycle 23's PER will measure about 141 ± 6 mo; hence, it will be a cycle of longer cycle length, like cycles 12–14 and 20 (the first new cycle spot was reported¹ in January 2008).

Inspection of figure 1 suggests that cycles 12–23 might be loosely grouped either into three arbitrary groups based on relative size (large-amplitude cycles (18, 19, 21, and 22), average-amplitude cycles (15, 17, 20, and 23), and small-amplitude cycles (12, 13, 14, and 16)) or possibly into two groups based on cycle length (short-period cycles (15–19, 21, and 22) and long-period cycles (12–14, 20, and 23)).¹⁵ Table 1 gives averages and standard deviations (in parentheses) for Rm , RM , ASC , and PER for each of these groupings. It is found that large-amplitude cycles tend to rise more quickly to RM (shorter ASC), be of shorter PER , and have higher Rms than average-size cycles, which in turn have higher/shorter values as compared to small-amplitude cycles. Likewise, short-period cycles tend to rise more quickly to RM and to have higher Rms and RMs than long-period cycles.

Figure 2 shows the mean cycle curve of the month-to-month rate of change in the smoothed monthly mean sunspot number (R), based on epoch analysis and cycles 12–23 (the smoothed thick line) for elapsed time in months from $E(Rm)$, $t=0$ –132 mo. The occurrence dates for each cycle's maximum positive rate of change during the ascending portion of the sunspot cycle are across the top, and the actual values of the maximum positive rate of change during the ascending portion of the sunspot cycle are to the upper right. The occurrence dates for each cycle's maximum negative rate of change during the descending portion of the sunspot cycle are at the bottom, and the actual values of the maximum negative rate of change during the descending portion of the sunspot cycle are to the lower right.

Based on the aforementioned groupings (amplitude and period), it is found that large-amplitude cycles tend to have higher rates of change both during the ascending (9.5(1.4)) and descending (−7.5(1.1)) portions of the sunspot cycle as compared to cycles of average size (6.7(1.3) and −5.2(0.3)) and cycles of smaller amplitude (4.7(1.1) and −4.7(0.9)). Also, cycles of shorter period tend to have higher rates of change during both the ascending (8.5(2.0)) and descending (−6.5(1.5)) portions of the sunspot cycle as compared to cycles of longer period (4.9(1.0) and −4.7(0.8)). The timing of the

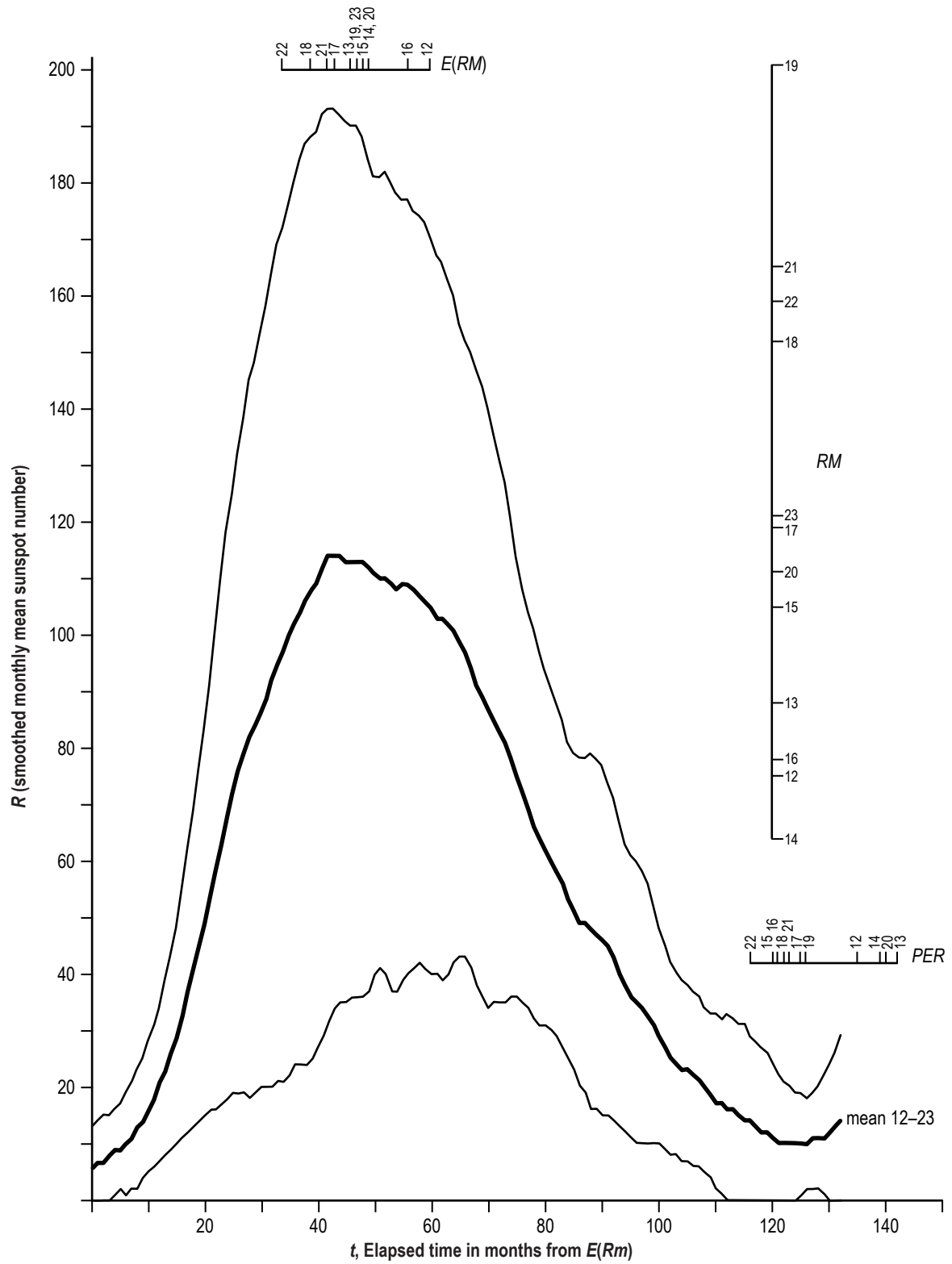


Figure 1. Variation of R for elapsed time in months $t = 0$ –132 mo from $E(Rm)$.

Table 1. Average parametric values for selected groupings of cycles.

Group	Cycles	$\langle Rm \rangle$	$\langle RM \rangle$	$\langle ASC \rangle$	$\langle PER \rangle^*$
Amplitude:					
Large	18, 19, 21, 22	8.9 (4.2)	169.0 (22.1)	40.5 (5.4)	121.8 (4.2)
Average	15, 17, 20, 23	5.6 (3.8)	114.0 (7.3)	46.8 (2.6)	128.3 (10.4)
Small	12-14, 16	3.9 (1.7)	76.2 (9.8)	52.8 (6.4)	134.3 (9.3)
Period:					
Short	15–19, 21, 22	6.6 (4.3)	139.8 (41.4)	44.1 (7.1)	121.9 (3.3)
Long	12–14, 20, 23	5.5 (3.3)	91.6 (23.8)	50.2 (5.6)	139.0 (2.9)

* Excludes Cycle 23

maximum positive rate of change in R (ΔR_{maxpos}) and the maximum negative rate of change of R (ΔR_{maxneg}) are found to span 14–42 and 51–83 mo, respectively, and to average 27.8 (10.1) and 71.4 (9.5) mo, respectively.

Figure 3 depicts the 12-mma of the month-to-month rate of change shown in figure 2. The thick line is the mean curve and the thin lines above and below the mean curve represent the 90-percent prediction limits. Smoothing removes a considerable amount of the choppiness that appears in figure 2. The occurrences of the 12-mma of ΔR_{maxpos} are across the top, the individual values of the 12-mma of ΔR_{maxpos} are to the upper right, the occurrences of the 12-mma of ΔR_{maxneg} are across the bottom, and the individual values of the 12-mma of ΔR_{maxneg} are to the lower right.

Based on the aforementioned groupings (amplitude and period), it is found that large-amplitude cycles tend to have higher rates of change both during the ascending (6.8(1.3)) and descending (−4.6(0.6)) portions of the sunspot cycle as compared to cycles of average size (3.9(0.3) and −3.0(0.4)) and small-amplitude cycles (2.7(0.6) and −2.3(0.5)). Also, cycles of shorter period tend to have higher rates of change during the ascending (5.5(1.9)) and descending (−3.8(1.2)) portions of the sunspot cycle as compared to cycles of longer period (3.1(0.8) and −2.6(0.7)). The timing of the 12-mma of ΔR_{maxpos} and ΔR_{maxneg} is found to span 14–41 and 66–96 mo, respectively, and is found to average 23.7 (7.8) and 76.8 (8.3) mo, respectively.

Figure 4 depicts the cyclic variation of the previously discussed parameters. The horizontal line in each subpanel is the mean. The standard deviation (sd) is also given. It is noticeable that cycles of late (cycles 18–23) have higher averages of Rm , RM , ΔR_{maxpos} , ΔR_{maxneg} , 12-mma of ΔR_{maxpos} and 12-mma of ΔR_{maxneg} as compared to earlier cycles (cycles 12–17), and the differences in their means are statistically important. Thus, cycles of late have been more robust than earlier cycles and the higher parametric values may result from a long-term secular increase over time.^{16,17}

Figure 5 shows the cyclic variation of specific timing parameters, where $t(1)$ is the elapsed time in months from $E(Rm)$ to the epoch of ΔR_{maxpos} ($E(\Delta R_{\text{maxpos}})$), $t(2)$ is the elapsed time in months from $E(\Delta R_{\text{maxpos}})$ to $E(RM)$, $t(3)$ is the elapsed time in months from $E(RM)$ to the epoch of ΔR_{maxneg} ($E(\Delta R_{\text{maxneg}})$), and $t(4)$ is the elapsed time in months from $E(\Delta R_{\text{maxneg}})$ to $E(Rm)$ of the next cycle. Figure 6 shows the same timing parameters but using the 12-mma values of ΔR_{maxpos} and ΔR_{maxneg} . In both figures, the horizontal lines are the means (given to the right in

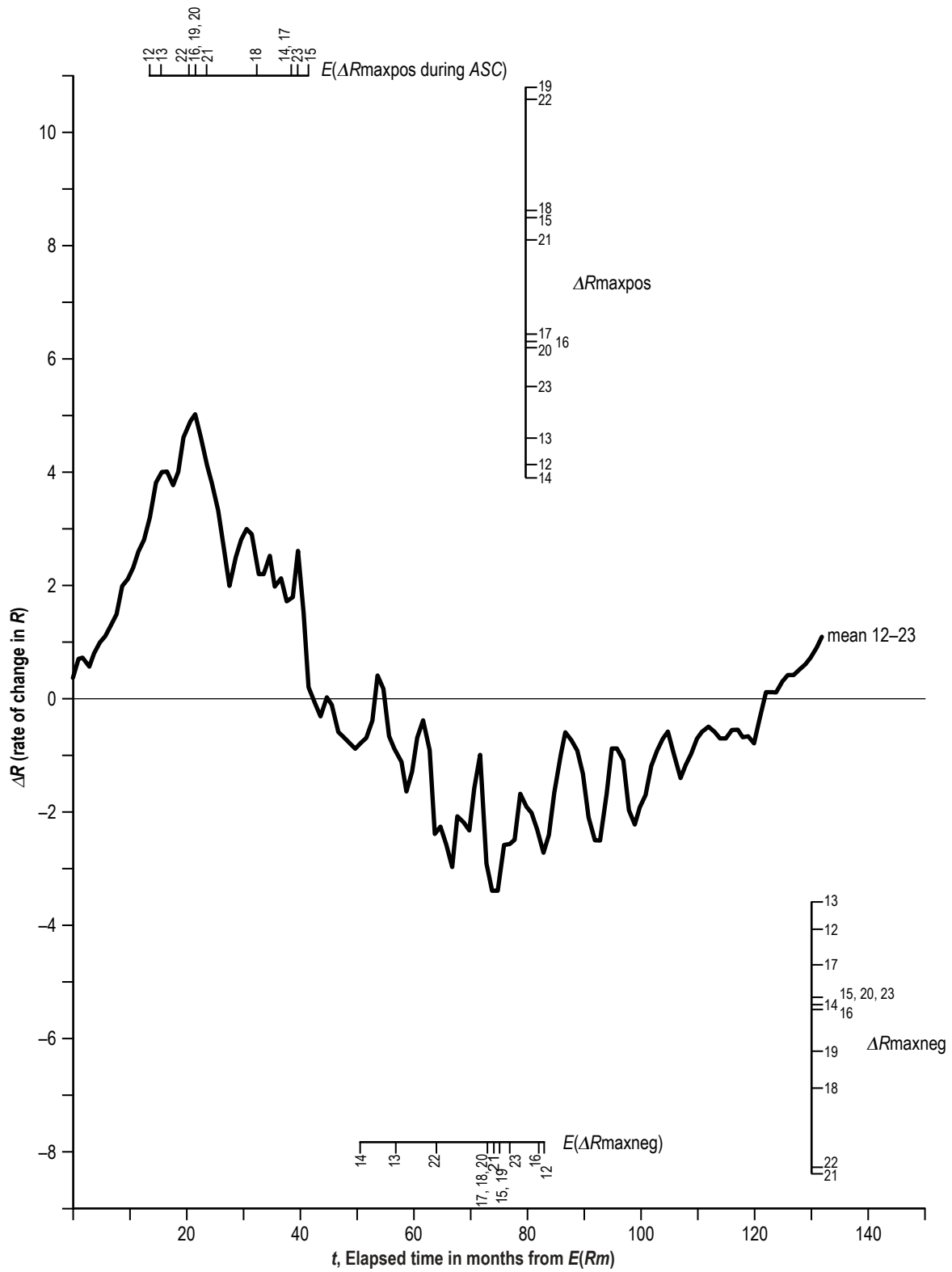


Figure 2. Variation of ΔR for elapsed time in months $t = 0$ –132 mo from $E(Rm)$.

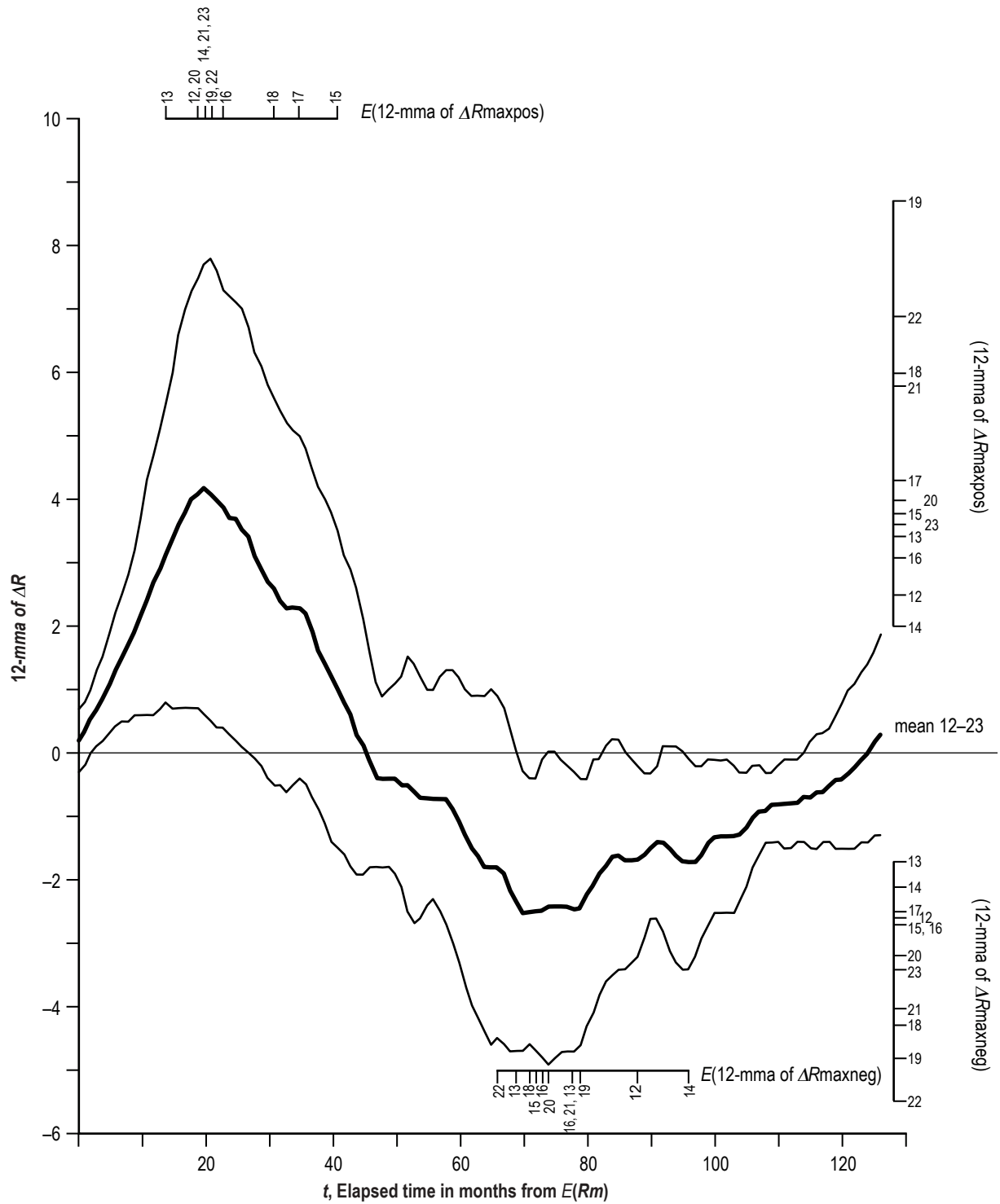


Figure 3. Variation of 12-mma of ΔR for elapsed time in months $t=0\text{--}126$ mo from $E(Rm)$.

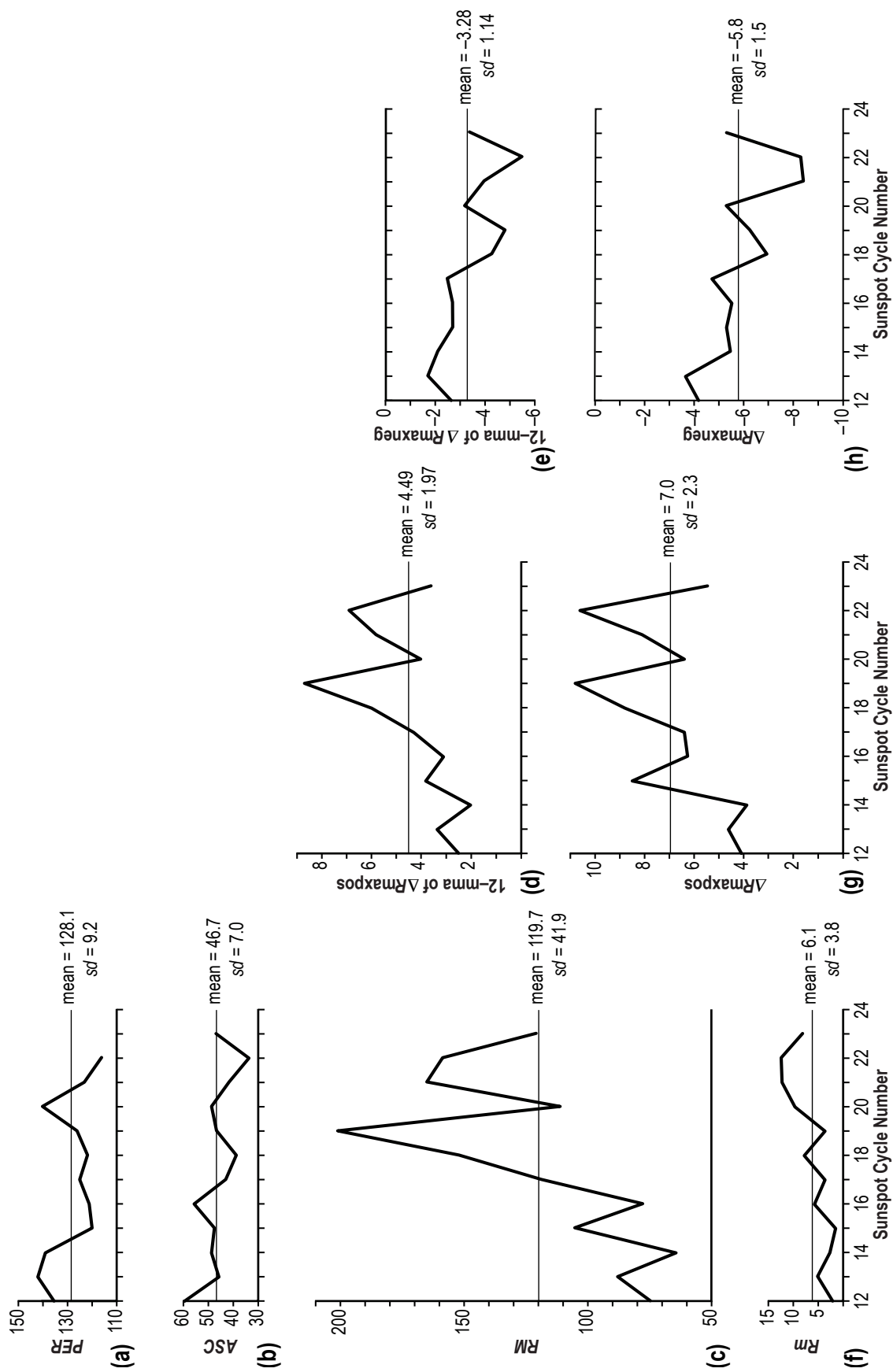


Figure 4. Variation of parametric values over cycles 12–23.

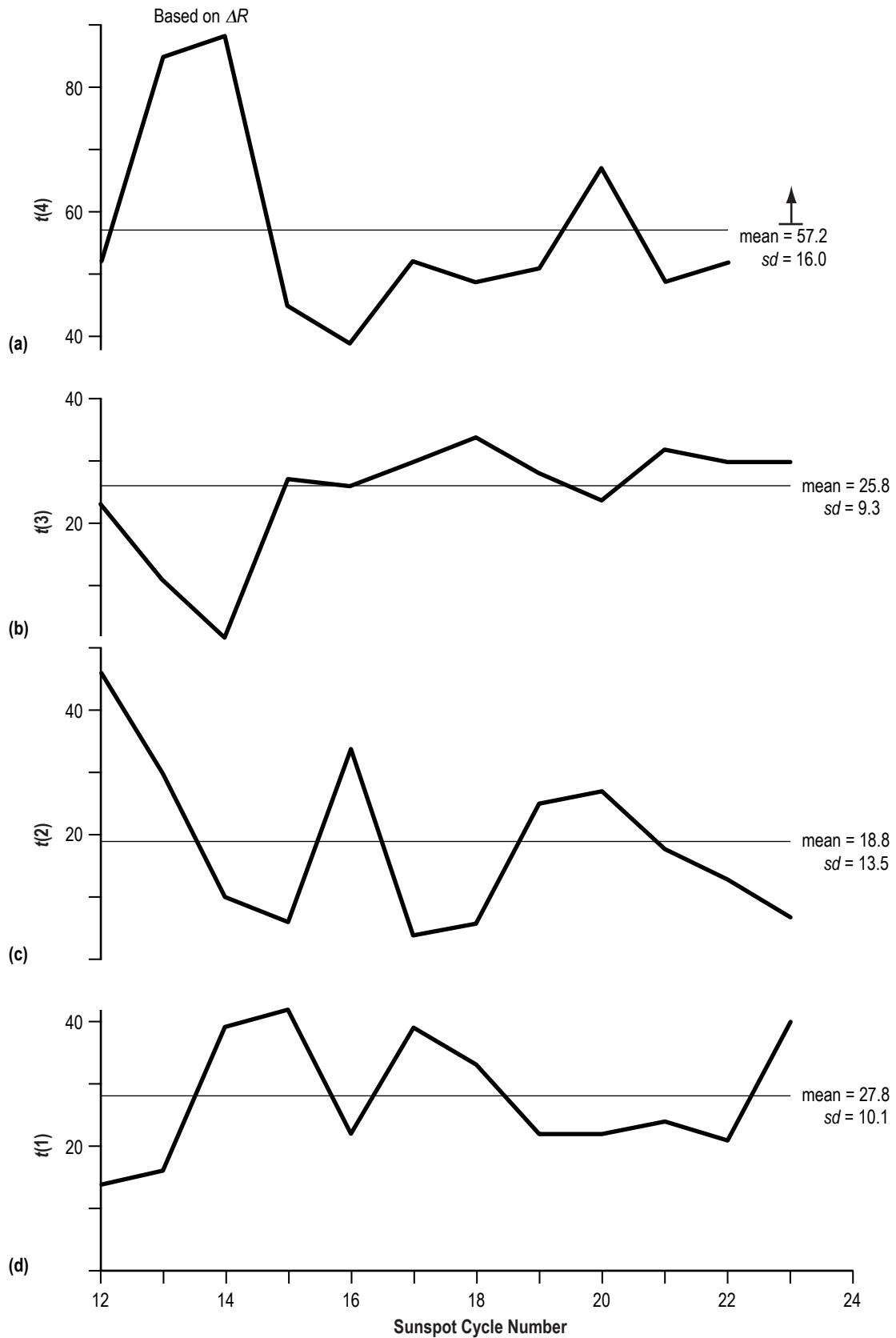


Figure 5. Variation of specific timing signatures based on ΔR .

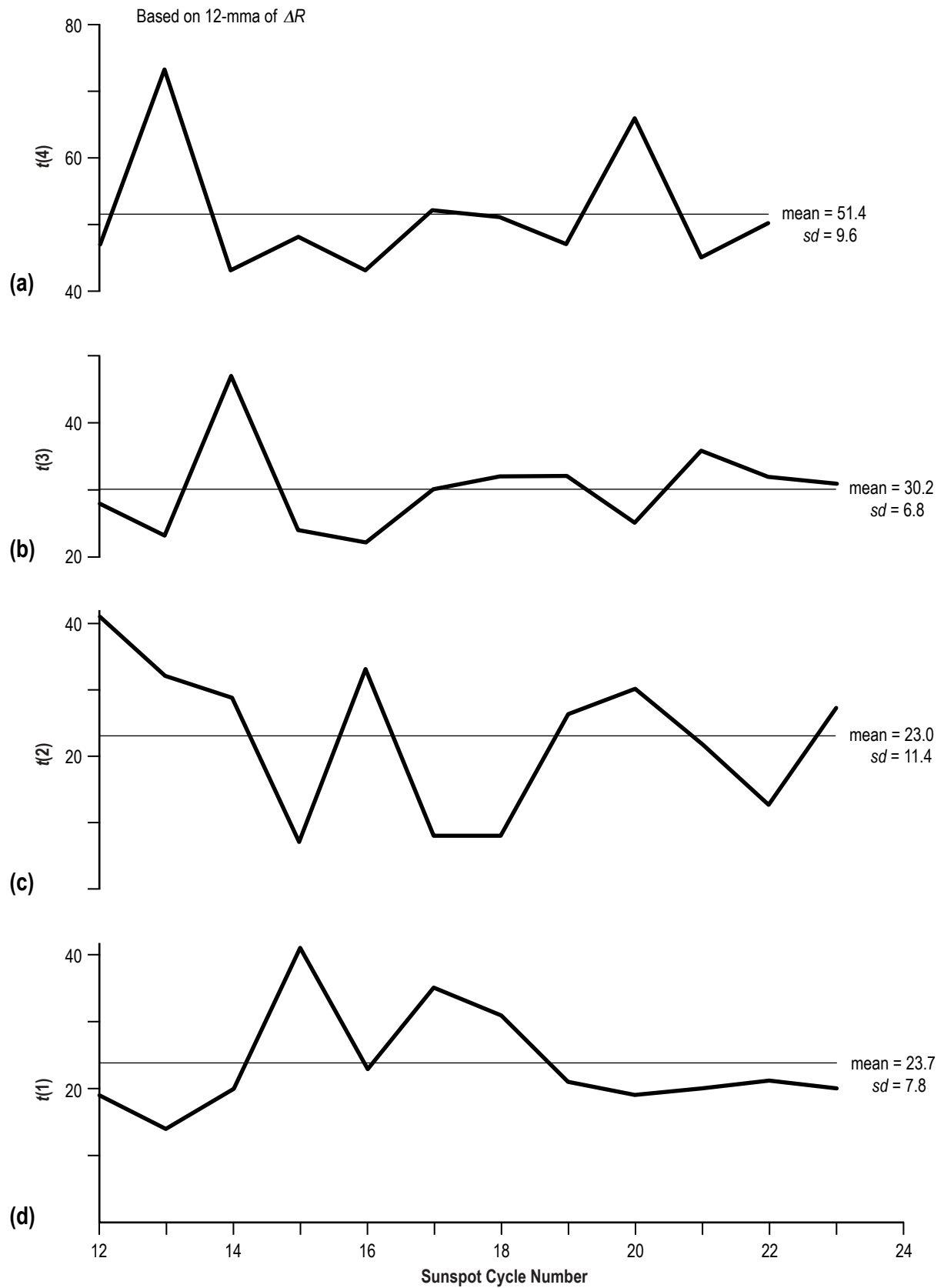


Figure 6. Variation of specific timing signatures based on 12-mma of ΔR .

each subpanel along with the sd). No significant differences in the timing parameters are apparent, comparing earlier cycles with those of late. Thus, on average, the greatest positive rate of growth in R occurs about 2 yr after Rm and about 1.5–2 yr before RM , and the greatest negative rate of growth in R occurs about 2–2.5 yr after RM and about 4–5 yr before succeeding cycle Rm . Table 2 provides a convenient summary of the cyclic parametric values and their occurrences relative to $E(Rm)$.

Table 2. Selected parametric values for sunspot cycles 12–23.

Cycle	$Rm(E(Rm))$	$RM(E(RM))$	ASC	PER	$\Delta Rmaxpos(t)$	$\Delta Rmaxneg(t)$	12-mma of $\Delta Rmaxpos(t)$	12-mma of $\Delta Rmaxneg(t)$
12	2.2 (12–1878)	74.6 (12–1883)	60	135	4.1 (14)	-4.1 (83)	2.47 (19)	-2.55 (88)
13	5.0 (03–1890)	87.9 (01–1894)	46	142	4.6 (16)	-3.6 (57)	3.36 (14)	-1.70 (69)
14	2.6 (01–1902)	64.2 (02–1906)	49	139	3.9 (39)	-5.4 (51)	2.00 (20)	-2.08 (96)
15	1.5 (08–1913)	105.4 (08–1917)	48	120	8.5 (42)	-5.3 (75)	3.82 (41)	-2.69 (72)
16	5.6 (08–1923)	78.1 (04–1928)	56	121	6.3 (22)	-5.5 (82)	3.07 (23)	-2.70 (78)
17	3.4 (09–1933)	119.2 (04–1937)	43	125	6.4 (39)	-4.7 (73)	4.25 (35)	-2.47 (73)
18	7.7 (02–1944)	151.8 (05–1947)	39	122	8.6 (33)	-6.9 (73)	5.95 (31)	-4.30 (71)
19	3.4 (04–1957)	201.3 (03–1958)	47	126	10.8 (22)	-6.2 (75)	8.69 (21)	-4.79 (79)
20	9.6 (10–1964)	110.6 (11–1968)	49	140	6.4 (22)	-5.3 (73)	3.97 (19)	-3.21 (74)
21	12.2 (06–1976)	164.5 (12–1979)	42	123	8.1 (24)	-8.4 (74)	5.83 (20)	-4.02 (78)
22	12.3 (09–1986)	158.5 (07–1989)	34	116	10.6 (21)	-8.3 (64)	6.92 (21)	-5.45 (66)
23	8.0 (05–1996)	120.8 (04–2000)	47	–	5.5 (40)	-5.3 (77)	3.57 (20)	-3.43 (78)

Recall from figure 4 that there is the hint that cycles of late have been more robust than earlier cycles and that this behavior may be the result of a long-term secular increase over time. Table 3 provides a convenient summary of the statistics, comparing parametric values against sunspot cycle number. Indeed, all parameters except PER appear to correlate well against sunspot cycle number. Table 3 gives the coefficient of linear correlation (r), the coefficient of determination (r^2) (a measure of the amount of variance explained by the regression), the y -intercept in the regression equation (a), the slope of the inferred regression (b), the standard error of estimate (se), and the confidence level (cl), where $cl > 95$ percent is considered statistically important ($cl > 90$ percent is of marginal statistical importance). Projections (90-percent prediction intervals) for cycle 24 based on the inferred regressions are also given. Hence, before cycle 24 has officially started, presuming the validity of the inferred regressions, cycle 24 is expected to have $Rm = 11.5 \pm 4.5$ (this will be exceeded low, for R measured 5.9 in September 2007), $RM = 166.9 \pm 64.1$, $ASC = 39.3 \pm 10.7$ mo, $\Delta Rmaxpos = 9.4 \pm 3.7$, $\Delta Rmaxneg = -7.6 \pm 2.0$, 12-mma $\Delta Rmaxpos = 6.55 \pm 3.03$, and 12-mma $\Delta Rmaxneg = -4.83 \pm 1.43$. Presuming cycle 23 has a $PER = 141$ mo (implying $E(Rm)$ for cycle 24 in March 2008), PER for cycle 24 is estimated to be about 125 ± 18 mo.

2.2 Correlative Results

2.2.1 $\Delta Rmaxpos$

The role of $\Delta Rmaxpos$ as a predictor for RM will be examined in this section. Figure 7 shows the scatter plot of RM versus $\Delta Rmaxpos$, where $\Delta Rmaxpos$ is recalled as the monthly $\Delta Rmaxpos$

Table 3. Correlations against sunspot cycle number.

Parameter	<i>r</i>	<i>r</i> ²	<i>a</i>	<i>b</i>	<i>se</i>	<i>cl</i> (%)	Cycle 24 (Predicted)**
<i>Rm</i>	0.780	0.608	-8.248	0.821	2.504	>99.5	11.5 ± 4.5
<i>RM</i>	0.594	0.353	20.868	6.085	35.375	>95	166.9 ± 64.1
ASC	-0.591	0.349	66.614	-1.140	5.902	>95	39.3 ± 10.7
<i>PER</i> *	-0.510	0.260	152.045	-1.409	8.306	<90	118.2 ± 15.2
ΔR_{maxpos}	0.558	0.312	0.620	0.364	2.029	>90	9.4 ± 3.7
ΔR_{maxneg}	-0.685	0.470	-0.806	-0.283	1.108	>98	-7.6 ± 2.0
12-mma of ΔR_{maxpos}	0.578	0.334	-1.031	0.316	1.674	>95	6.55 ± 3.03
12-mma of ΔR_{maxneg}	-0.746	0.556	0.861	-0.237	0.789	>99.5	-4.83 ± 1.43

*Excludes cycle 23 (presuming *PER* = 141 for cycle 23, then the numbers are, respectively, -0.223, 0.050, 139.446, -0.587, 9.663, <90, and 125.3 ± 17.5)

**90-percent prediction interval

(growth in *R*) during the ascending portion of the sunspot cycle (the ascending inflection point). The number beside each of the filled circles identifies the specific sunspot cycle. As an example, cycle 19 (the uppermost filled circle) had its greatest positive change in *R* ($= 10.8$) between $t = 22$ ($R = 98.5$) and $t = 23$ ($R = 109.3$) and it is this number that has been correlated with its later occurring *RM* ($= 201.3$). The thick straight line (denoted *y*) is the inferred regression line and the thin vertical and horizontal lines are the medians for the two parameters. The inferred regression is computed as $y = 11.365 + 15.519x$ and has $r = 0.867$, yielding $r^2 = 0.755$ (meaning that about three-fourths of the variance in *RM* can be explained by the inferred regression based on the behavior of ΔR_{maxpos}), and $se = 21.8$. The regression is found to be statistically significant at better than the 0.1-percent level of significance (or *cl* >99.9 percent). The result of Fisher's exact test for 2×2 contingency tables is also given,¹⁸ which indicates that the probability (*P*) of obtaining the observed result, or one more suggestive of a departure from independence (chance), is $P = 12.1$ percent. It is apparent then that by monitoring the month-to-month rate of change in *R*, the later occurring *RM* can be continually estimated. For $\Delta R_{\text{maxpos}} \leq 6.4$, it is anticipated that $RM \leq 121$; for $\Delta R_{\text{maxpos}} > 6.4$, it is anticipated that $RM > 105$.

Instead of using ΔR_{maxpos} as the estimator for the later occurring *RM*, *RM* can be compared against the slope at ΔR_{maxpos} , where the slope is computed as *R* at $E(\Delta R_{\text{maxpos}})$ minus *Rm* divided by the elapsed time in months between $E(\Delta R_{\text{maxpos}})$ and $E(Rm)$. Figure 8 displays the scatter plot of *RM* versus the slope at $E(\Delta R_{\text{maxpos}})$. As before, the number beside the filled circles identifies the sunspot cycle number, the thick line is the inferred regression, the thin lines are the medians, and the results of linear regression analysis and Fisher's exact test for the 2×2 contingency table are given. As an example, cycle 19 (the uppermost filled circle) had $\Delta R_{\text{maxpos}} = 10.8$ occurring at $t = 22$ mo. The slope for cycle 19 is then computed to be $(98.5 - 3.4)/22 = 4.32$, and it is this number that is correlated with the later-occurring *RM* ($= 201.3$).

Clearly, figure 8 provides a much-improved prediction of *RM* as compared to using figure 7 because of the large reduction in *se* (reduced by half, from 21.8 to 10.6), but not knowing exactly when ΔR_{maxpos} occurs presents a problem. For example, cycles 14, 15, 17, and 23 had their actual ΔR_{maxpos} values very late in their ascents ($t = 39, 42, 39$, and 40 mo, respectively),

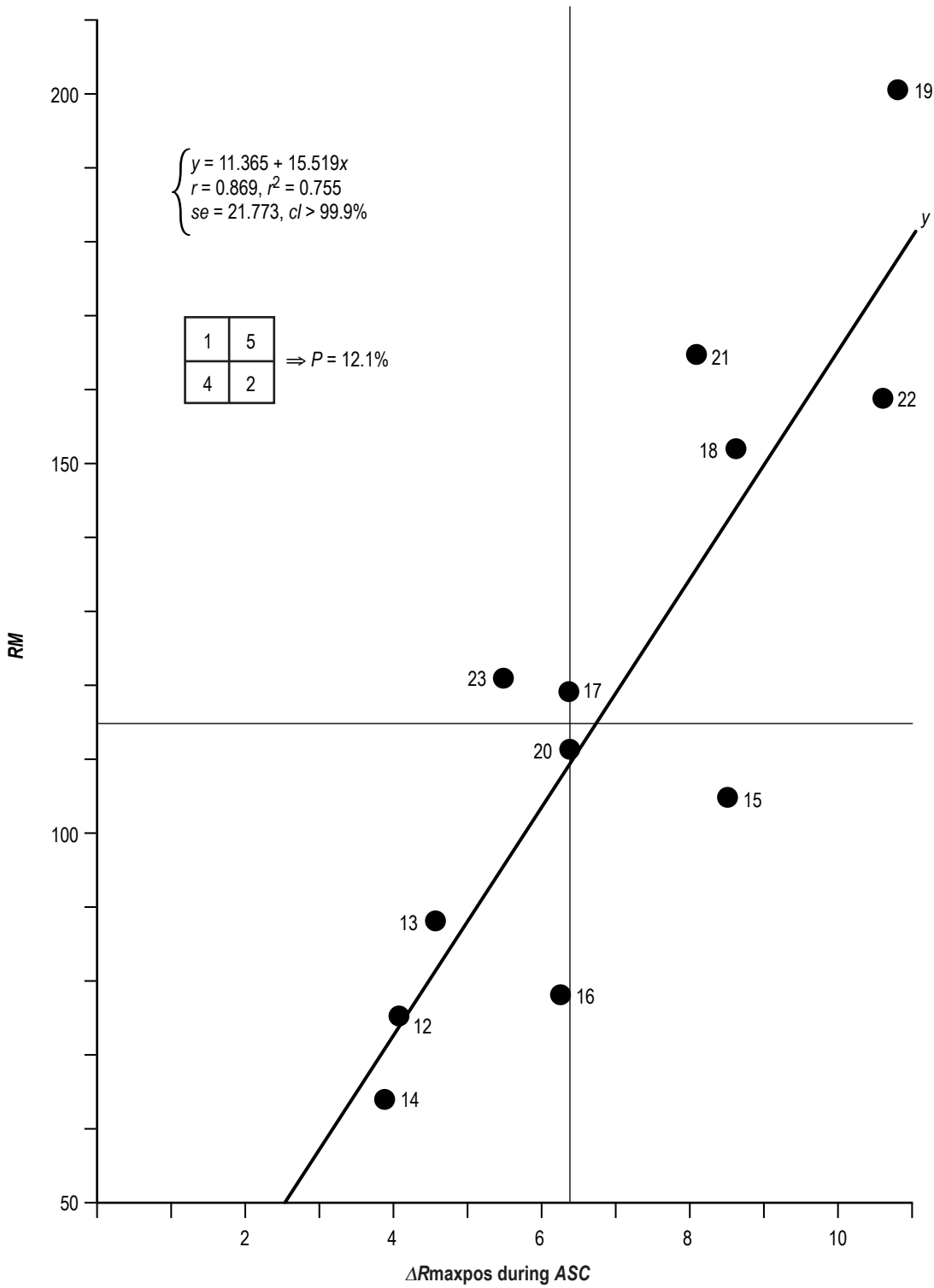


Figure 7. Scatter plot of RM versus ΔR_{maxpos} .

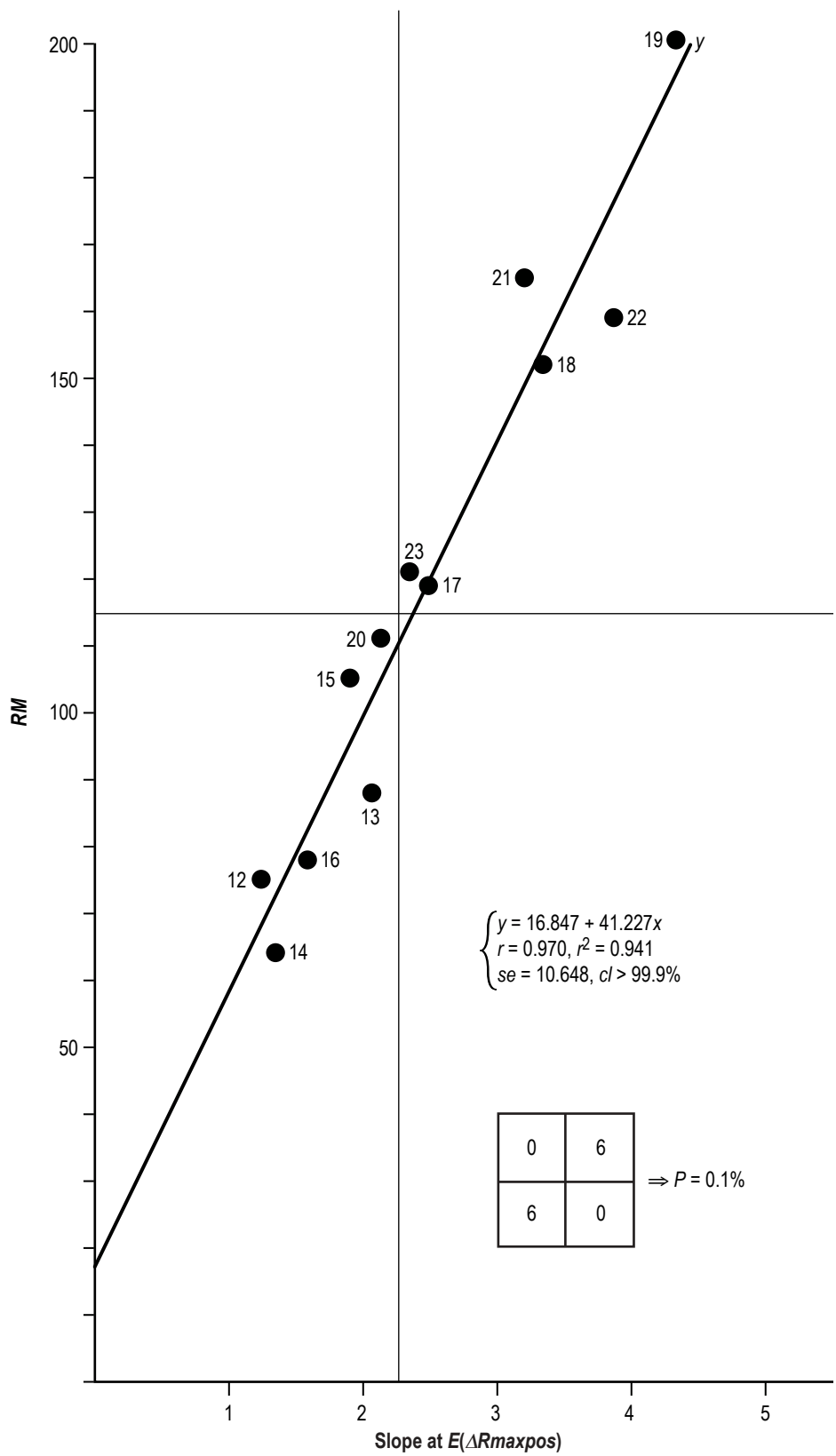


Figure 8. Scatter plot of RM versus slope at $E(\Delta R_{\text{maxpos}})$.

although smaller local peaks occurred earlier in their ascents (3.2 at $t=16$ and 3.5 at $t=30$ for cycle 14, 5.4 at $t=17$ for cycle 15, 4.8 at $t=24$ and 5.4 at $t=33$ for cycle 17, and 5.2 at $t=20$ for cycle 23). Using these earlier values, cycle 14's RM would have been predicted to be about 61 (at $t=16$) and 66 (at $t=30$), both values very close to its actual $RM=64$; cycle 15's RM would have been predicted to be about 95 (at $t=17$), close to but below its actual $RM=105$; cycle 17's RM would have been predicted to be about 86 (at $t=24$) and 95 (at $t=33$), both close to but below its actual $RM=119$; and cycle 23's RM would have been predicted to be about 92 (at $t=20$), close to but below its actual $RM=121$. Because the 90-percent prediction intervals associated with each predicted RM is ± 39.5 , all of the actual RM values would have fallen within the prediction interval.

Instead, using the estimated slope at the time of the earlier peaks, it would have been predicted that cycle 14's RM to be about 60 (at $t=16$) and 72 (at $t=30$), cycle 15's RM to be about 84 (at $t=17$), cycle 17's RM to be about 91 (at $t=24$), and cycle 23's RM to be about 91 (at $t=20$). Because the 90-percent prediction intervals associated with each predicted RM is ± 19.3 , only the actual RM values for cycles 14 and 15 would have fallen within the prediction interval; cycles 17 and 23 would have fallen just outside the upper limit of the prediction interval (by about 10 units of sunspot number).

Because many of the cycles either had their ΔR_{maxpos} or alternative early cycle local peaks before $t=30$, it may be that RM can be predicted on the basis of the collective behavior of ΔR_{maxpos} in comparison to RM before $t=30$ mo. Figure 9 shows the variation of the r^2 s determined month-by-month from $E(R_m)$ based on a comparison of RM and the month-to-month change in $R(\Delta R)(t)$ for $t=0-26$ mo. It is found that the peak r^2 occurs at $t=25$ mo; although, as early as $t=14$ mo, $\Delta R(t)$ provides a statistically meaningful estimate for RM (the earliest estimate appears to be at $t=10$ mo, but it has a rather large se , equal to ± 34 mo). In figure 9, the cross-hatched pattern signifies those t s when a statistically meaningful correlation is inferred between RM and $\Delta R(t)$.

Figure 10 displays the scatter plots of RM versus $\Delta R(t=10)$ (panel (a)) and $\Delta R(t=25)$ (panel (b)). Clearly, by monitoring $\Delta R(t)$, an increasingly accurate estimate for RM can be effected, especially at $t=25$ mo. Such an approach would have suggested its RM would likely be about 105.6 ± 33.6 (the 90-percent prediction interval) for cycle 23.

2.2.2 12-mma of ΔR

The role of the 12-mma of ΔR as a predictor for RM will be examined in this section. Figure 11 shows the scatter plot of RM versus the maximum positive value of the 12-mma of ΔR . The structure of the chart follows that used in figures 7, 8, and 10. Figure 11 is strikingly similar to figure 8, both having $r=0.97$, $r^2=0.94$, and $se=10.6$. Thus, by monitoring the 12-mma of ΔR , increasingly accurate predictions of the later occurring RM can be effected. The disadvantage of the 12-mma of $\Delta R(t)$ as compared to $\Delta R(t)$ is that it lags that of $\Delta R(t)$ by several months, so its use as a predictor of RM appears more appropriately to be that of a confirmatory role.

Figures 12 and 13 are equivalents to figures 9 and 10, but based on the comparison of RM versus the 12-mma of $\Delta R(t)$. From figure 12, it is found that as early as $t=8$ mo, the value of the 12-mma of $\Delta R(t)$ provides a statistically meaningful estimate for RM , with the best predictor

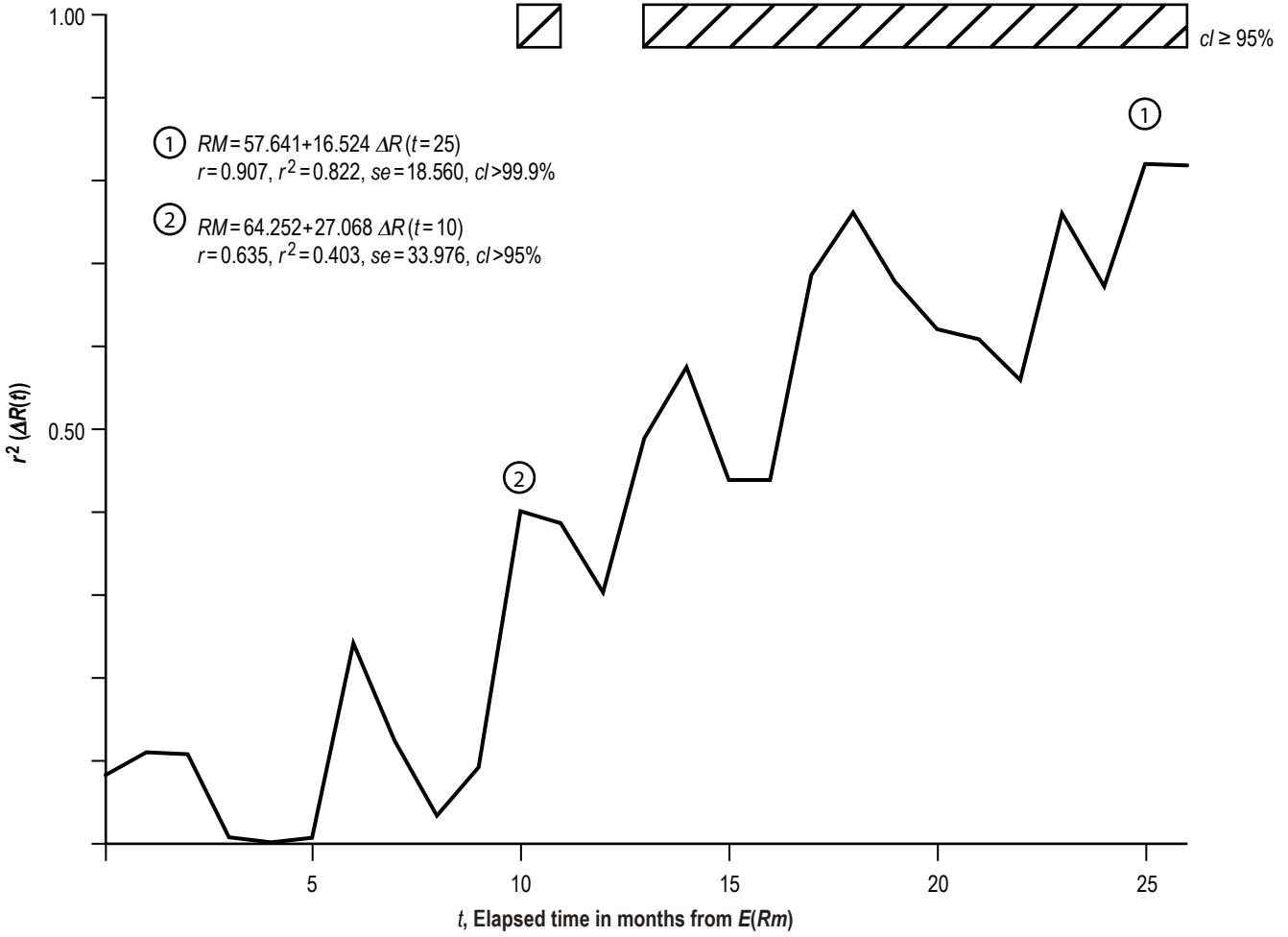


Figure 9. Variation of $r^2(\Delta R(t))$.

occurring at $t=22$ mo. For cycle 23, such an approach would have suggested its RM likely would be 111.3 ± 25.8 (the 90-percent prediction interval).

2.2.3 ΔR_{maxneg}

The role of ΔR_{maxneg} as a predictor of PER for the current cycle and of Rm and RM for the following cycle will be examined in this section. Figure 14 displays the scatter plot of PER versus ΔR_{maxneg} . The structure of the chart follows that of previous charts. Based on Fisher's exact test for 2×2 contingency tables, it is found that the P of obtaining the observed result, or one more suggestive of a departure from independence (chance), is $P=17.5$ percent. Based on linear regression analysis, a statistically important correlation is inferred to exist between PER and ΔR_{maxneg} , having $r=0.66$, $r^2=0.44$, $se=7.2$, and $cl > 95$ percent. From the known value of ΔR_{maxneg} for cycle 23 ($= -5.3$ at $t=77$ mo or 30 mo past $E(Rm)$), it is inferred that PER for cycle 23 should be about 130 ± 13 mo (the 90-percent prediction interval). Thus, on the basis of the validity of the inferred regression, it is noted that there is only a 5-percent chance that cycle 23 will persist longer than 143 mo, indicating $E(Rm)$ for cycle 24 should be expected before May 2008.

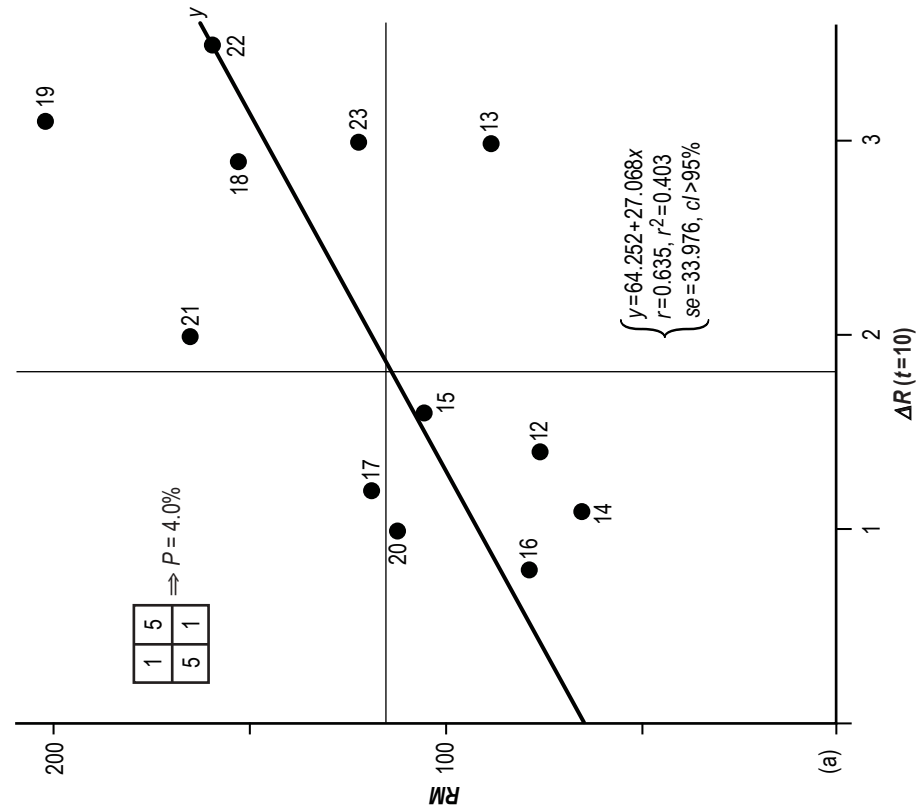
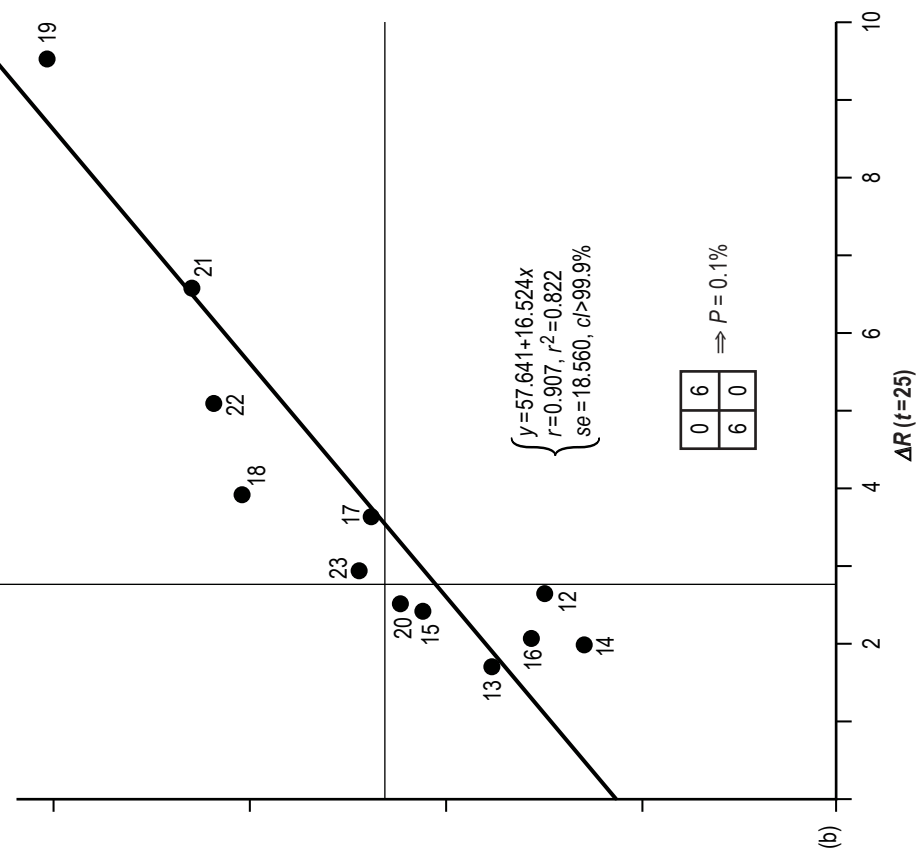


Figure 10. Scatter plots of RM versus $\Delta R(t = 10)$ and RM versus $\Delta R(t = 25)$.



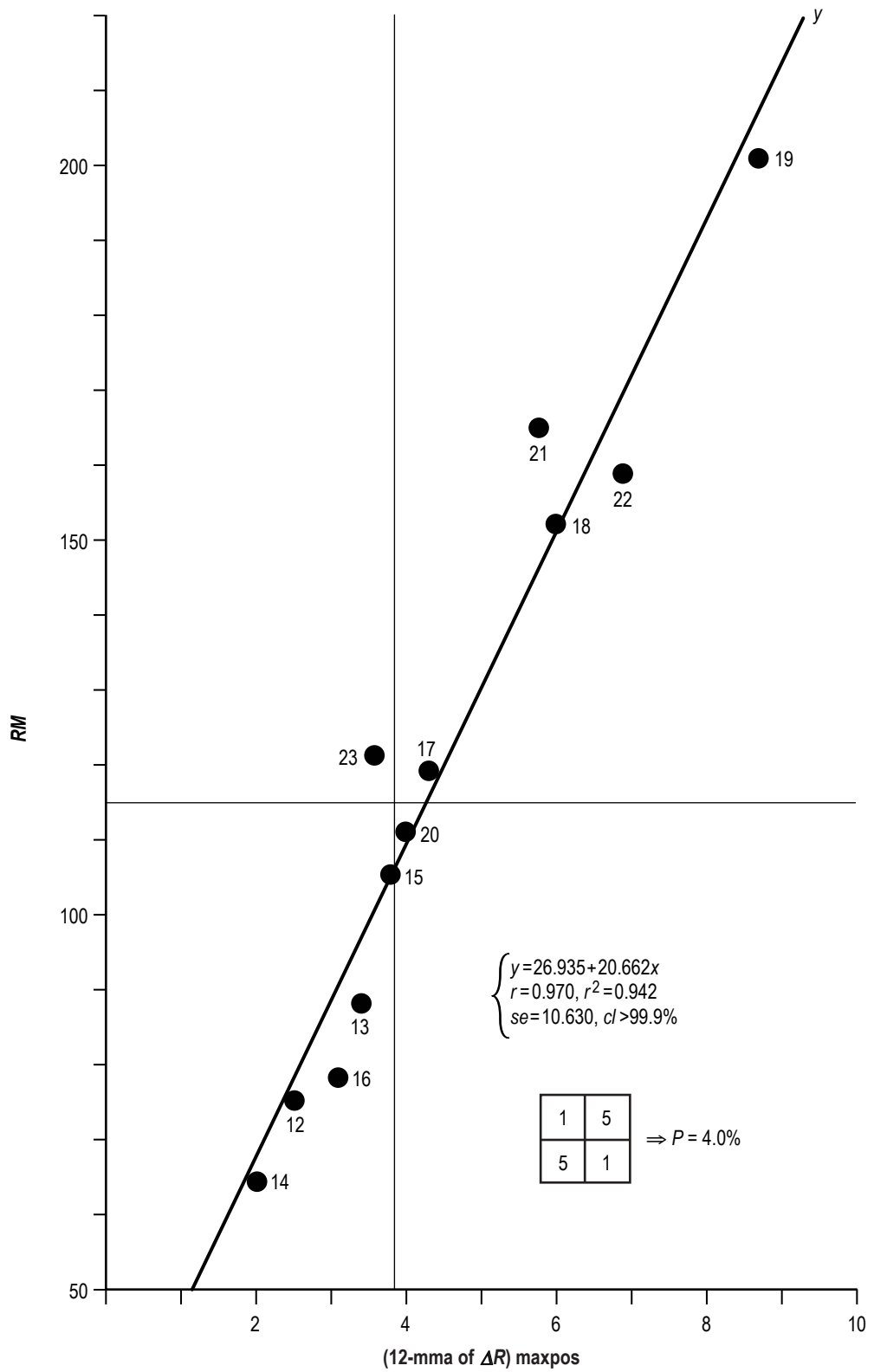


Figure 11. Scatter plot of RM versus $(12\text{-mma of } \Delta R) \text{ maxpos}$.

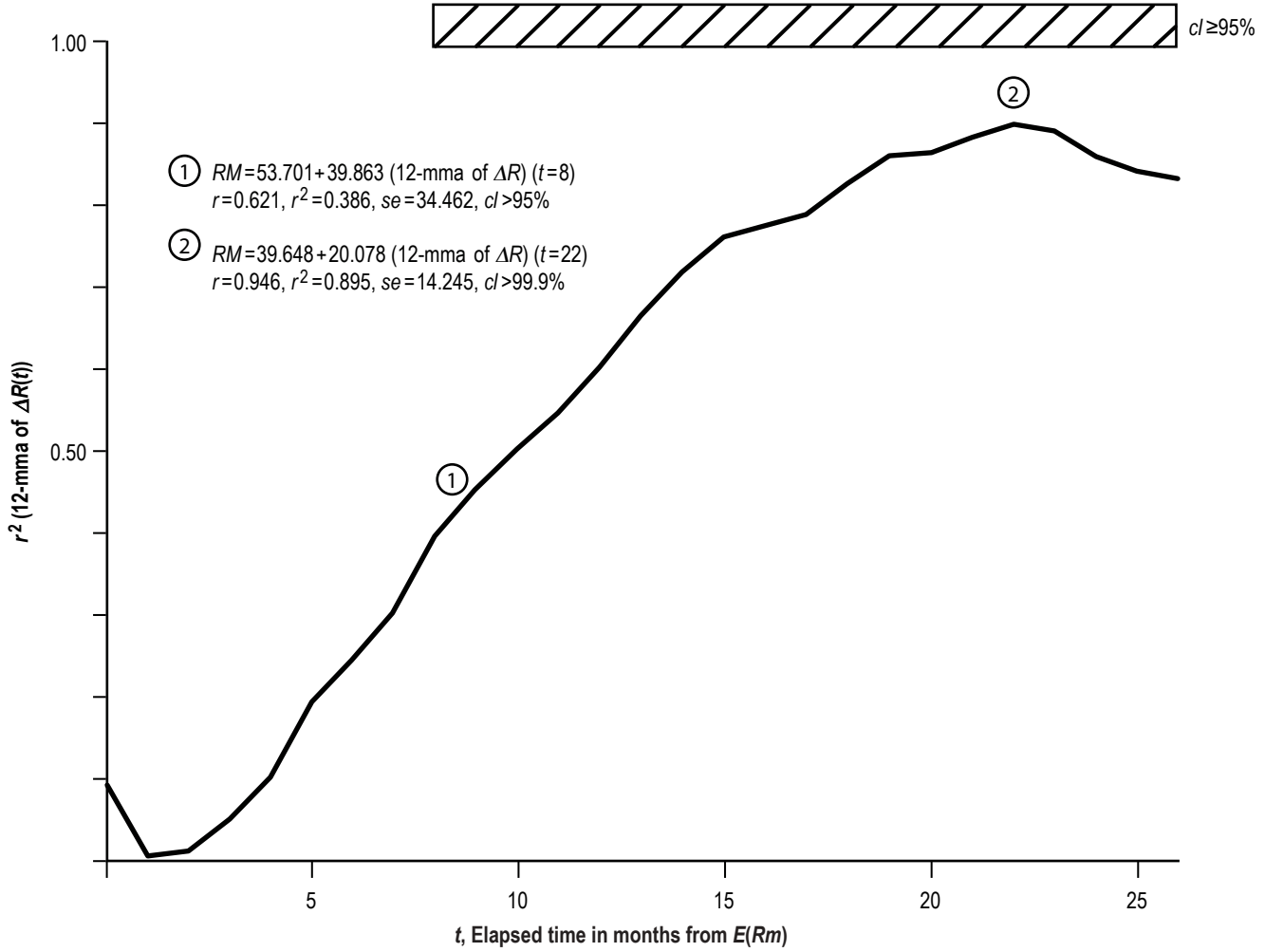


Figure 12. Variation of r^2 (12-mma of $\Delta R(t)$).

Figures 15 and 16 show scatter plots of $Rm(n+1)$ and $RM(n+1)$ versus ΔR_{maxneg} , respectively. Neither plot is inferred to be statistically important. Thus, while ΔR_{maxneg} seems to provide an indication for the expected length of an ongoing cycle, it does not provide any indication as to the expected size of the Rms and RM s for the following cycle.

2.2.4 (12-mma of ΔR)maxneg

The role of (12-mma of ΔR)maxneg as a predictor of PER for the current cycle and of Rm and RM for the following cycle will be examined in this section. Figure 17 displays the scatter plot of PER versus (12-mma of ΔR)maxneg. As found for PER versus ΔR_{maxneg} (fig. 14), a statistically important correlation is inferred between PER and (12-mma of ΔR)maxneg, having $r=0.63$, $r^2=0.39$, $se=7.5$, and $cl>95$ percent. From the known value of (12-mma of ΔR)maxneg for cycle 23 ($= -3.43$ at $t=78$ mo or 31 mo past $E(RM)$), it is inferred that PER for cycle 23 will be about 127 ± 14 mo (the 90-percent prediction interval). Thus, on the basis of the inferred regression, there is only a 5-percent chance that cycle 23 will persist longer than 141 mo, indicating $E(Rm)$ for cycle 24 should be expected before April 2008.

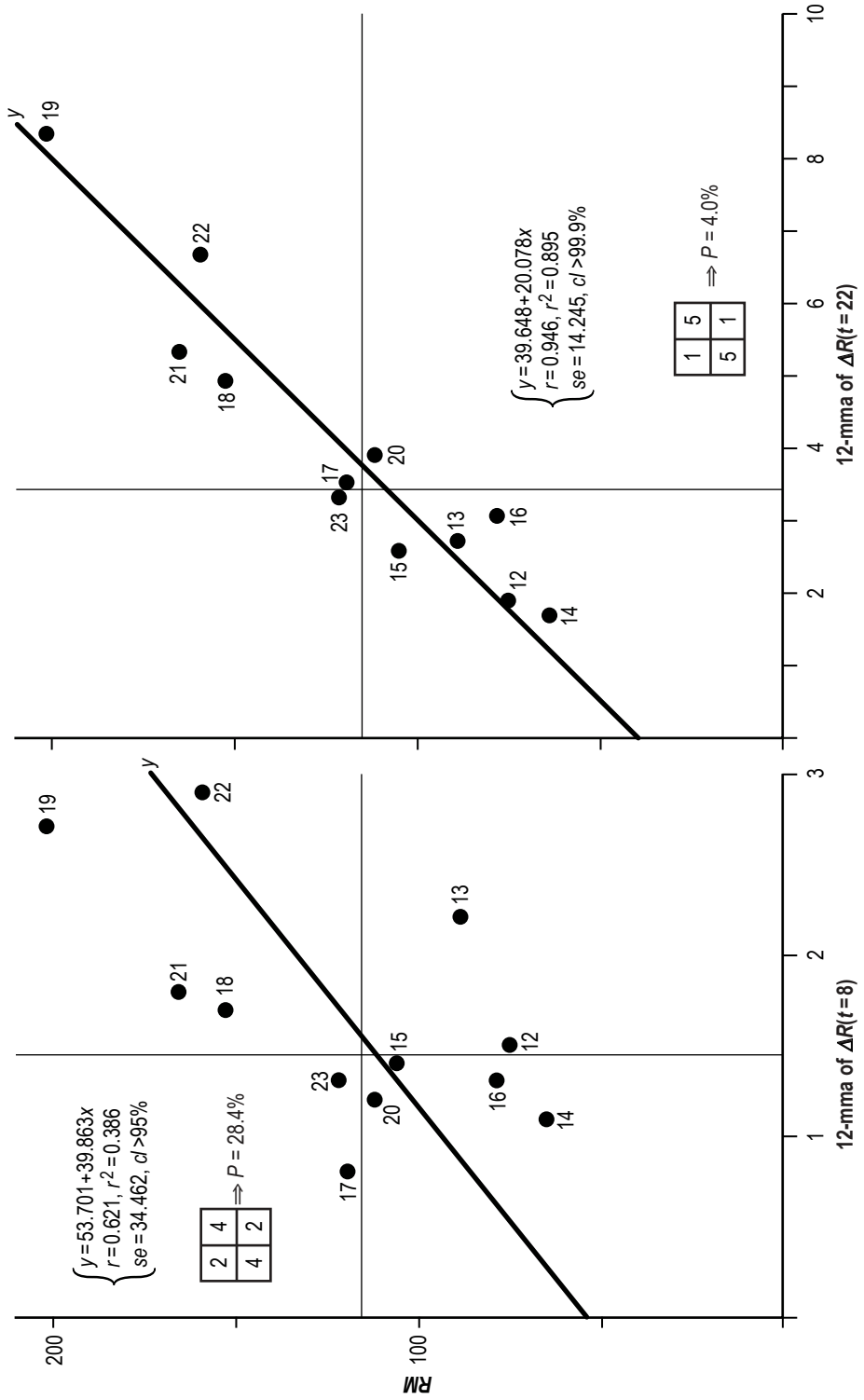


Figure 13. Scatter plots of RM versus 12-mma of $\Delta R(t = 8)$ and RM versus 12-mma of $\Delta R(t = 22)$.

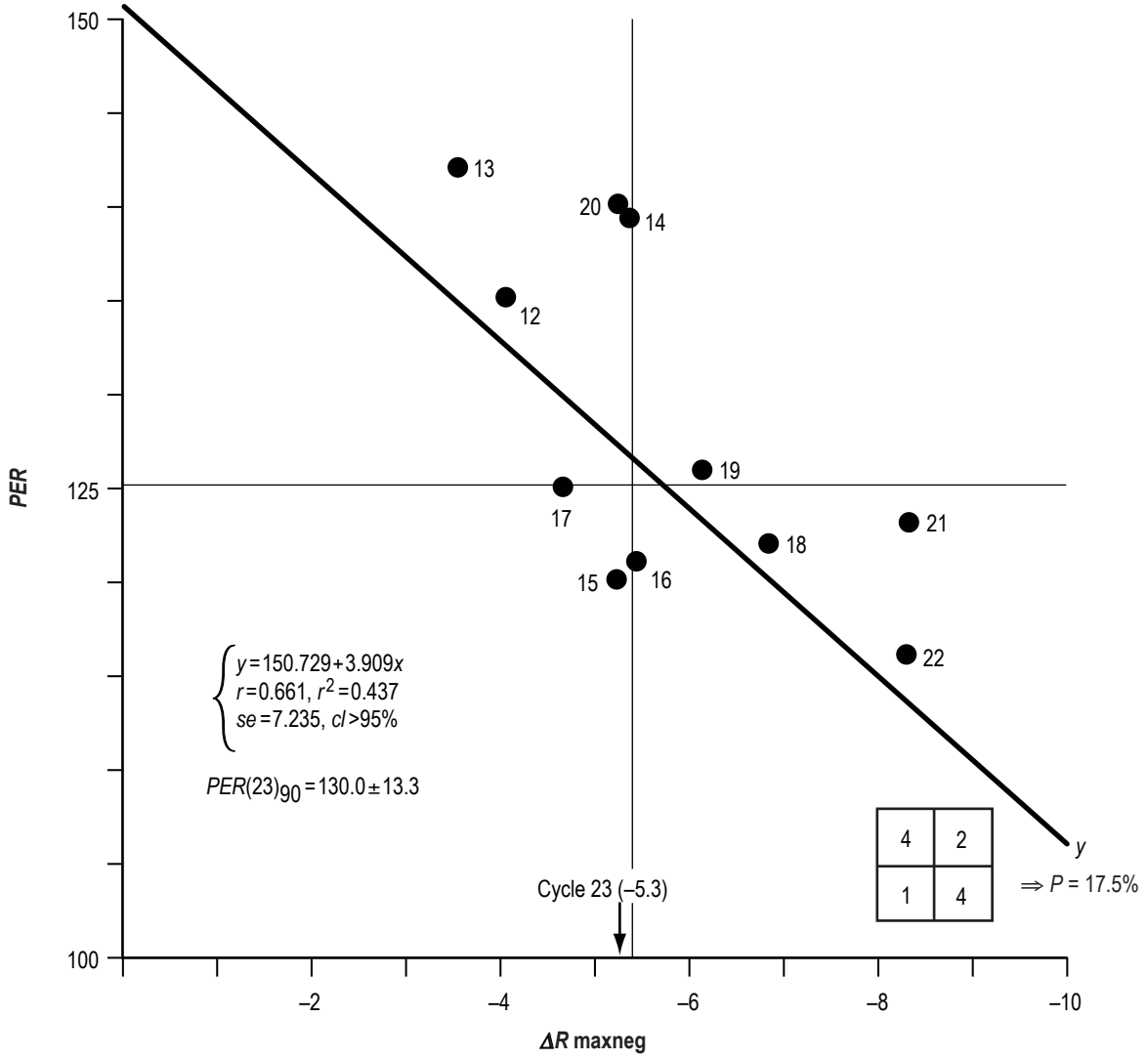


Figure 14. Scatter plot of PER versus ΔR maxneg.

Figures 18 and 19 show scatter plots of $Rm(n+1)$ and $RM(n+1)$ versus (12-mma of ΔR) maxneg, respectively. Neither plot is inferred to be statistically important. Thus, while (12-mma of ΔR)maxneg seems to provide an indication for the expected length of an ongoing cycle, it does not provide any indication as to the size of the Rms and RMs of the following cycle.

2.2.5 $\Delta R(T)$ and 12-mma of $\Delta R(T)$

The roles of $\Delta R(T)$ and 12-mma of $\Delta R(T)$ for elapsed times in months from $E(RM)$, T , as predictors of PER , $Rm(n+1)$, and $RM(n+1)$ will be examined in this section. Figure 20 shows the scatter plots of PER versus $\Delta R(T=30)$ (panel (a)) and PER versus 12-mma of $\Delta R(T=31)$ (panel (b)). The two plots represent the best fits of PER versus $\Delta R(T)$ and PER versus 12-mma of $\Delta R(T)$ for $T=0$ –40 mo. Apparently, the reason for the success of these inferred regressions is the fact that $\Delta R(T)$ and the 12-mma of $\Delta R(T)$ are near their maximum negative values at these

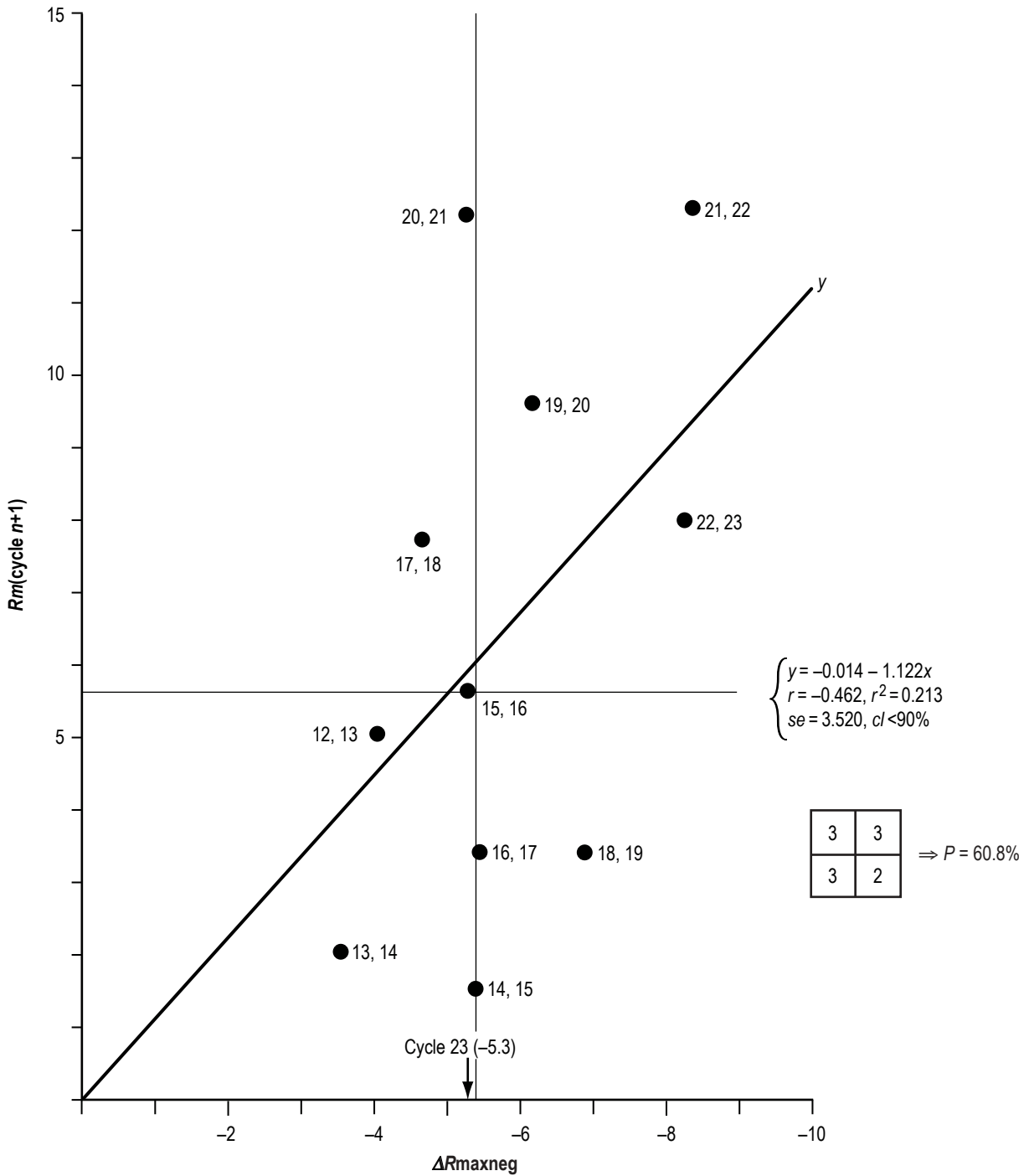


Figure 15. Scatter plot of $R_m(\text{cycle } n + 1)$ versus ΔR_{maxneg} .

elapsed times relative to $E(RM)$. Both fits are statistically important. Based on the known value of $\Delta R(T=30)$ during the descending portion of cycle 23 ($= -5.3$), it is inferred that its PER will be about 122 ± 14 mo (the 90-percent prediction interval). Based on the known value of the 12-mma of $\Delta R(T=31)$ during the descending portion of cycle 23 ($= -3.43$), it is inferred that its PER will

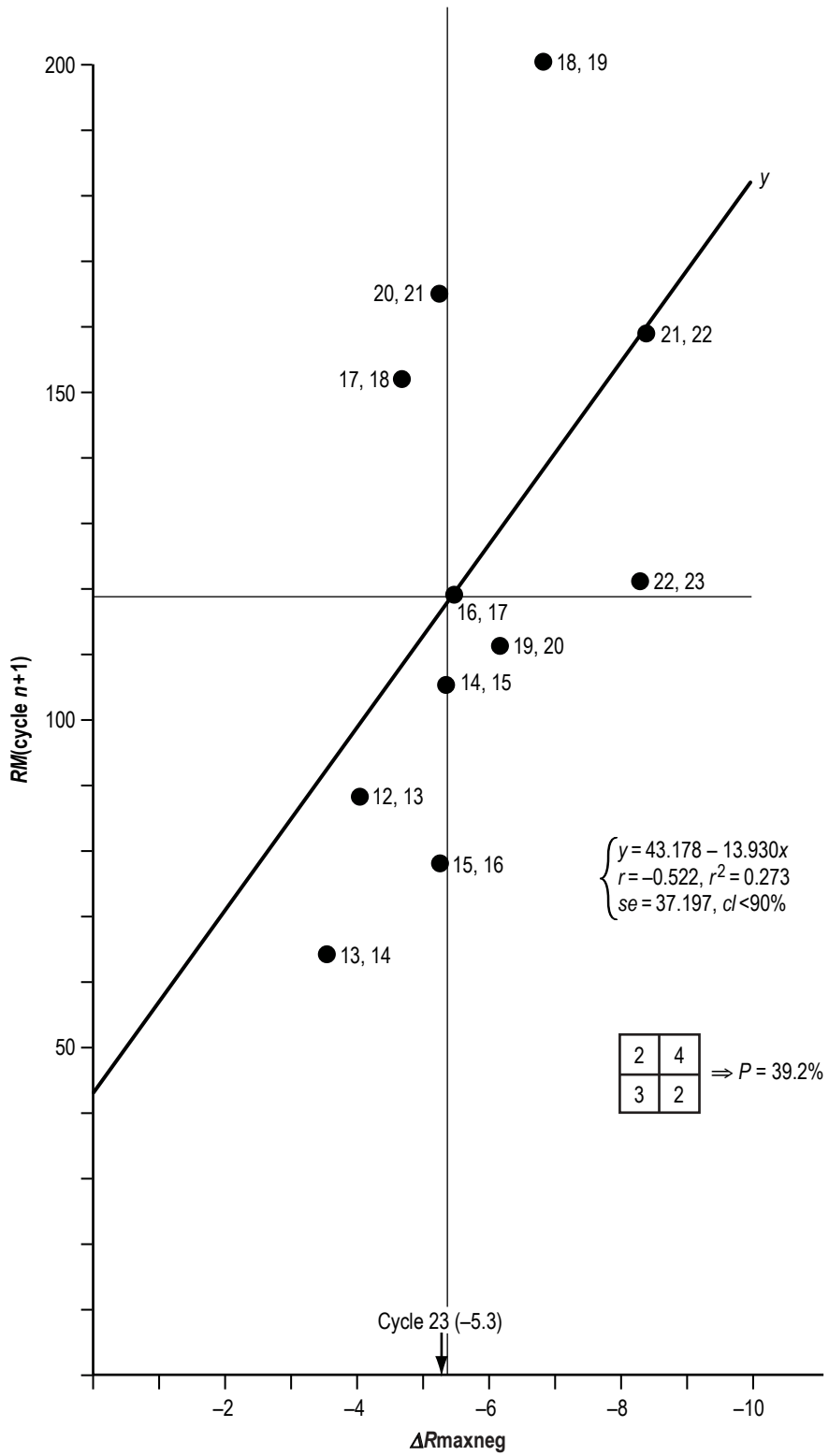


Figure 16. Scatter plot of $RM(\text{cycle } n+1)$ versus ΔR_{maxneg} .

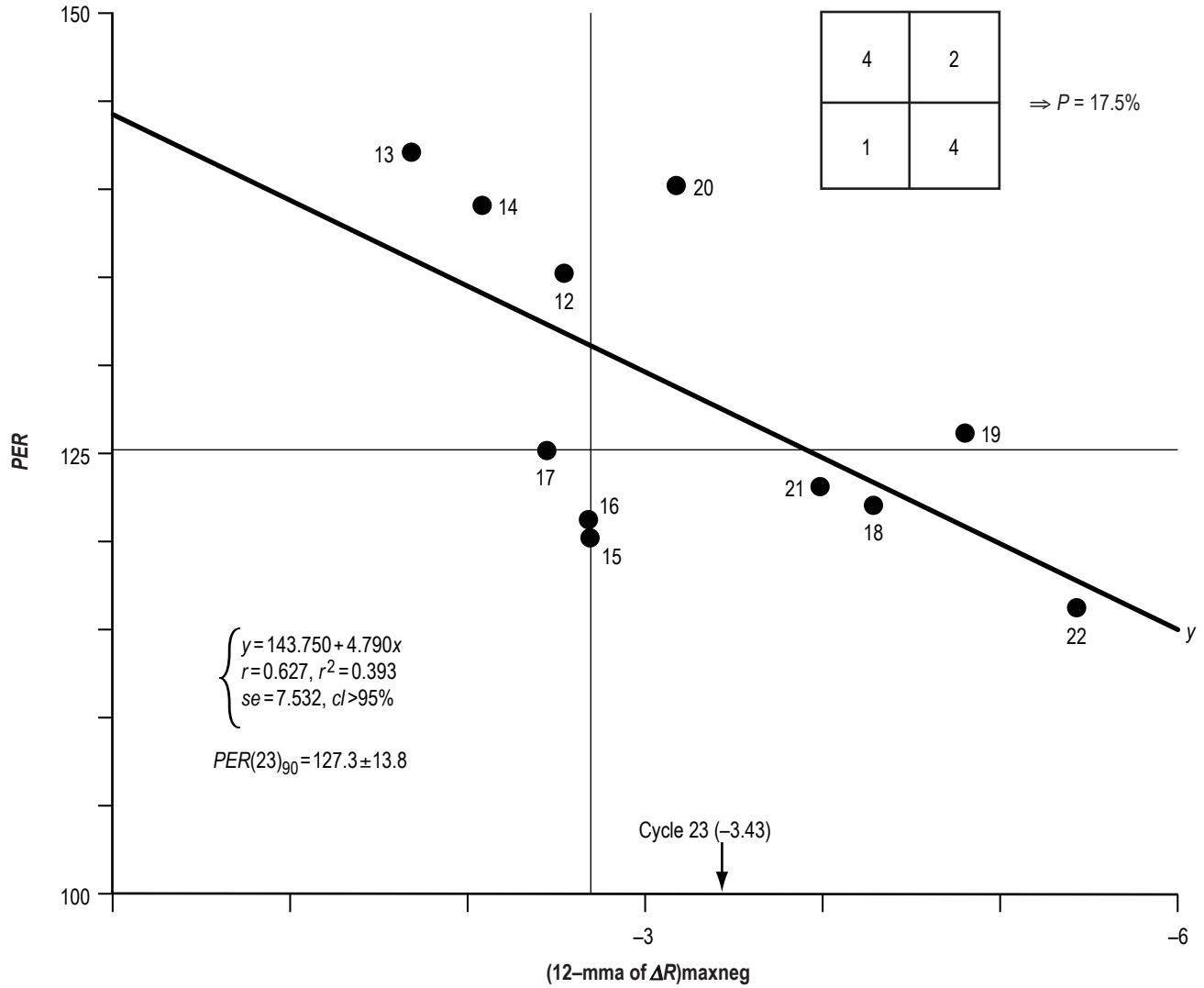


Figure 17. Scatter plot of *PER* versus $(12\text{-mma of } \Delta R)\text{maxneg}$.

be about 125 ± 12 mo (the 90-percent prediction interval). Since cycle 23 has already persisted for 135 mo, $E(Rm)$ should be expected very soon. However, because new cycle spots typically occur either simultaneously with up to several months prior to $E(Rm)$ and because the first confirmed new cycle spot for cycle 24 occurred in January 2008, it appears that $E(Rm)$ for cycle 24 will occur outside these 90-percent prediction intervals. (The interval from May 1996–August 2007 corresponds to 135 mo. Because cycle 23 undoubtedly will have a *PER* more like cycles 12–14 and 20 rather than cycles 15–19, 21, and 22, inclusion of cycle 23's *PER* will greatly weaken the inferred regressions. Hence, the inferred correlations are probably a fluke, with cycles more likely distributed preferentially as short- and long-period cycles, rather than following the inferred linear regression lines.)

Figure 21 shows the scatter plots of $Rm(n+1)$ versus $\Delta R(T=31)$ (panel (a)) and $Rm(n+1)$ versus 12-mma of $\Delta R(T=27)$ (panel (b)), the most statistically important correlations. While the first plot (panel (a)) is only of marginal statistical importance ($cl > 90$ percent), the latter one

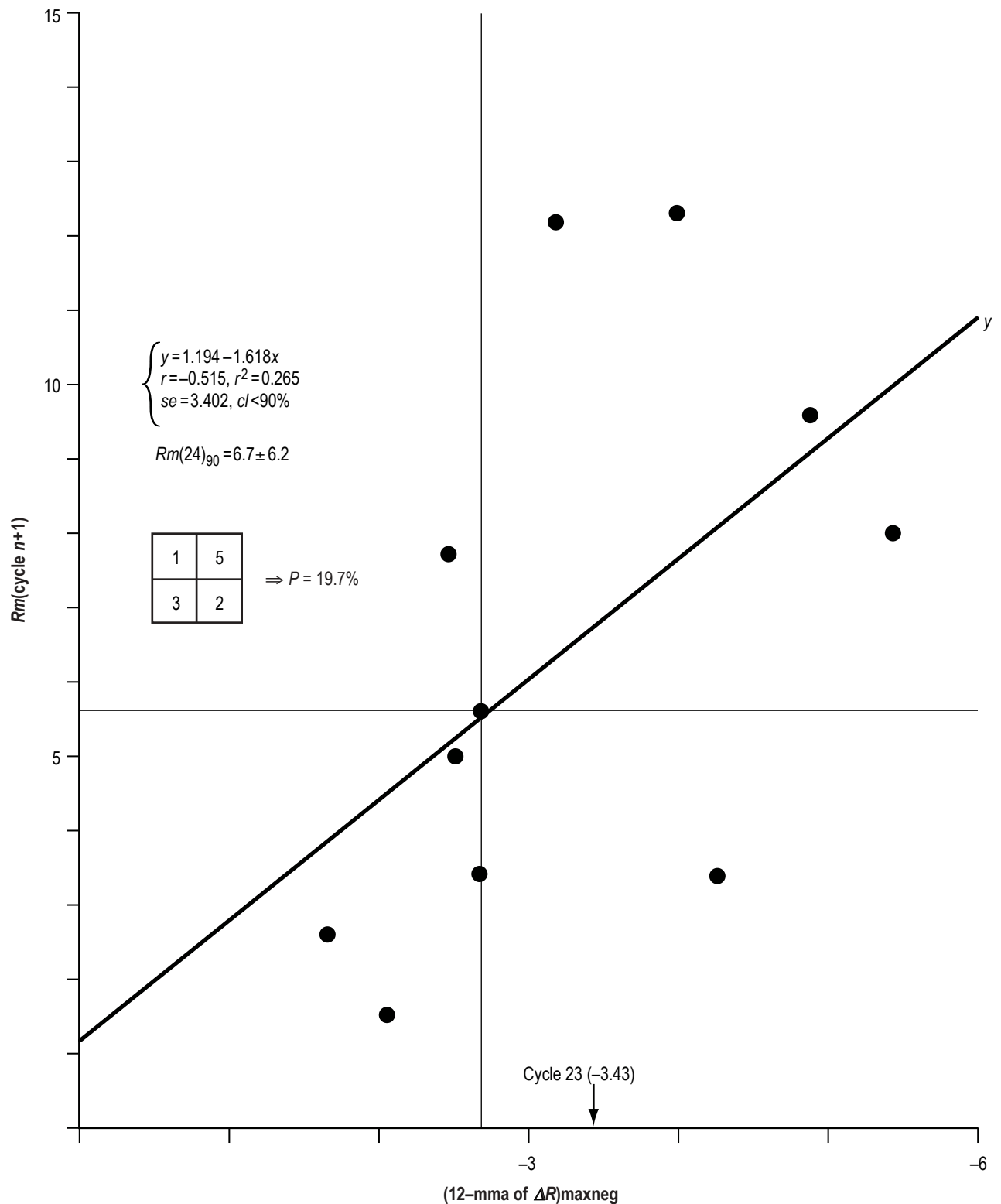


Figure 18. Scatter plot of $Rm(\text{cycle } n + 1)$ versus $(12\text{-mma of } \Delta R)\text{maxneg}$.

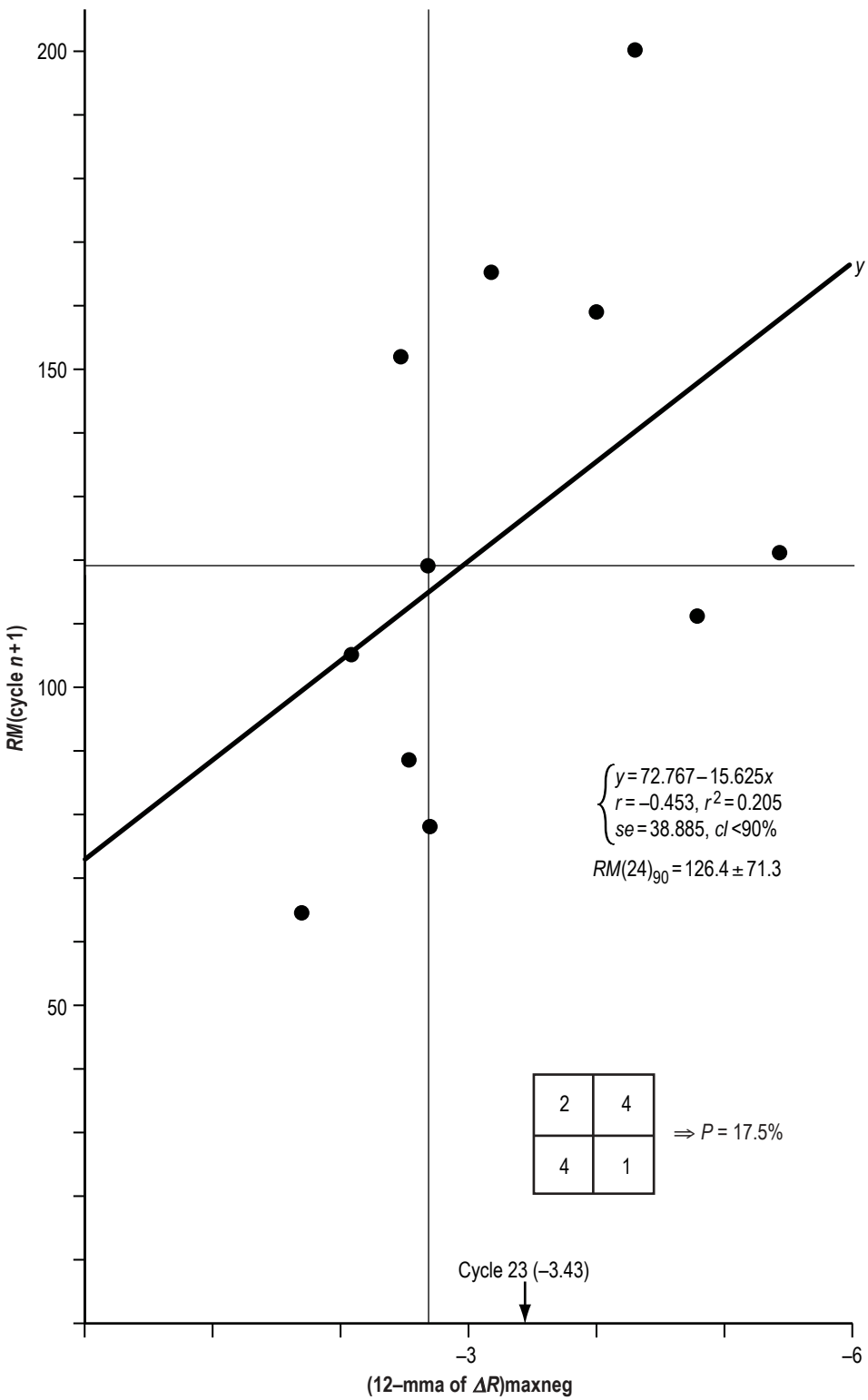


Figure 19. Scatter plot of $RM(\text{cycle } n + 1)$ versus $(12\text{-mma of } \Delta R)\text{maxneg}$.

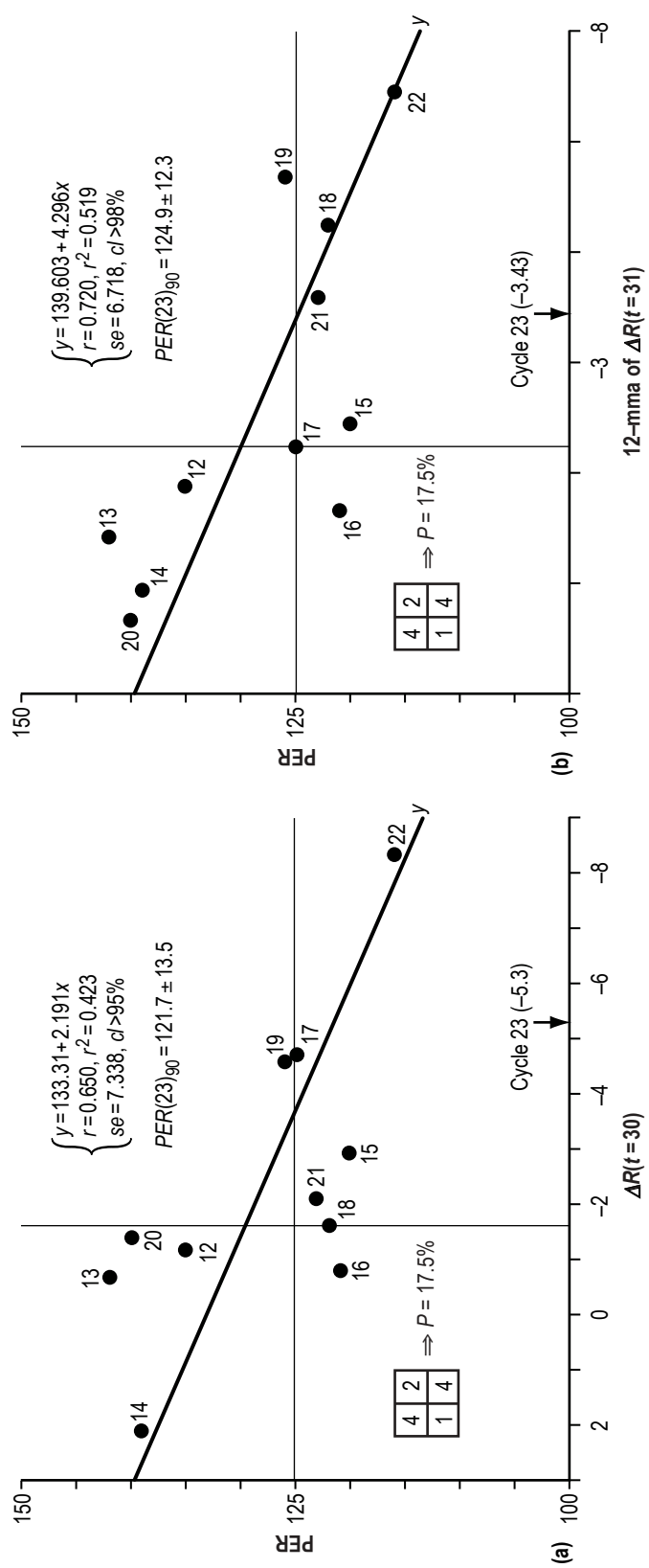


Figure 20. Scatter plots of PER versus $\Delta R(T=30)$ and 12-mma of $\Delta R(T=31)$.

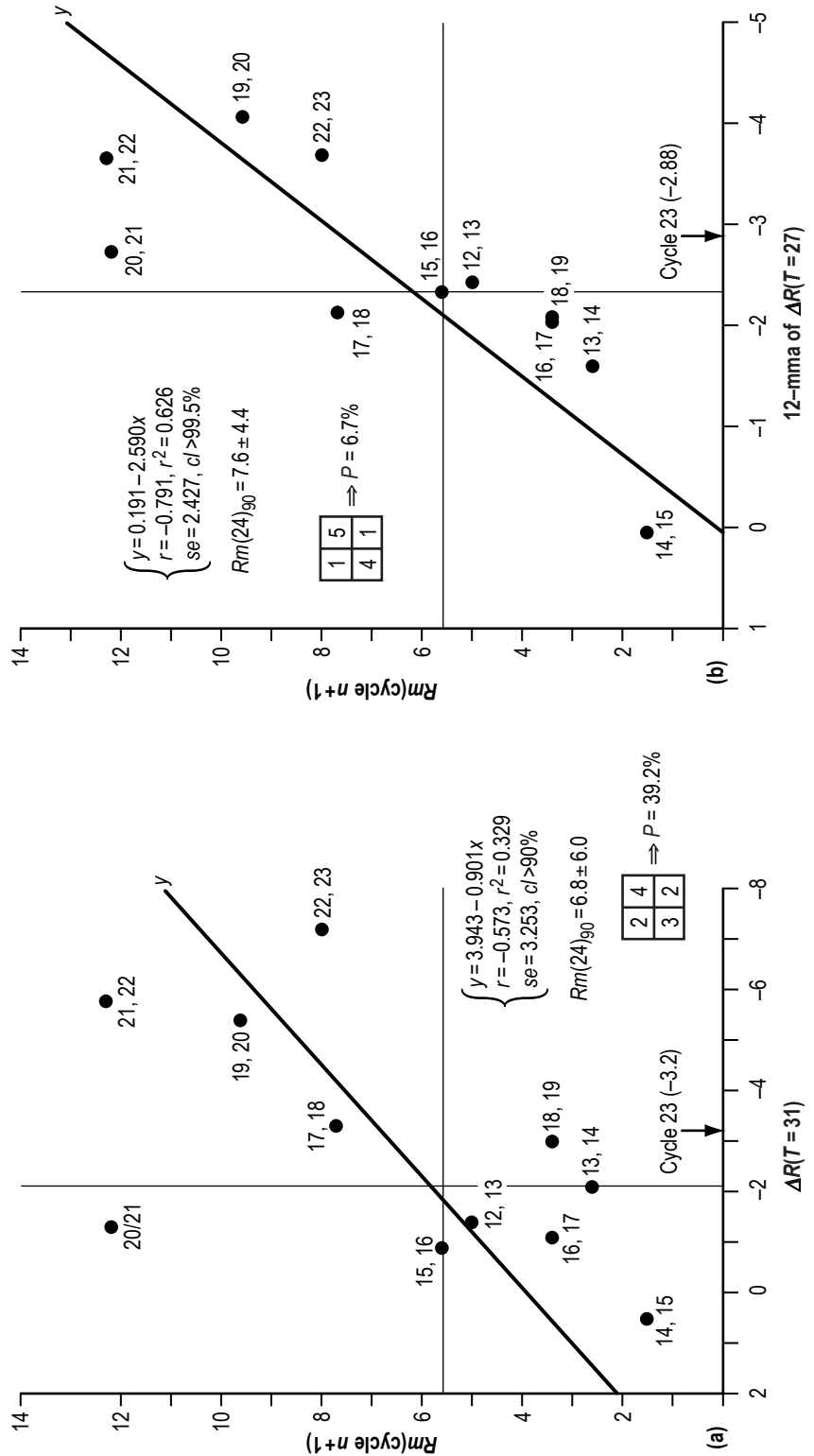


Figure 21. Scatter plots of $Rm(\text{cycle } n + 1)$ versus $\Delta R(T = 31)$ and 12-mma of $\Delta R(T = 27)$.

(panel (b)) is found to be highly statistically important ($cl > 99.5$ percent). Based on the known value ($= -3.2$) of cycle 23's $\Delta R(T=31)$, the Rm for cycle 24 is estimated to be about 7 ± 6 (the 90-percent prediction interval); while, based on the known value ($= -2.88$) of cycle 23's 12-mma of $\Delta R(T=27)$, the Rm for cycle 24 is estimated to be about 8 ± 4 (the 90-percent prediction interval). Based on the 2×2 contingency table, $Rm(24)$ can be expected to be ≥ 5.6 . The lowest value of the 12-mma of R observed to date during the declining portion of cycle 23 measures 5.9 (September 2007), so obviously $E(Rm)$ for cycle 24 is most imminent.

Attempts to find a statistically important correlation between $RM(n+1)$ and $\Delta R(T)$ and between $RM(n+1)$ and the 12-mma of $\Delta R(T)$ proved fruitless. However, for completeness sake, figure 22 is included, which shows the scatter plots of $RM(n+1)$ versus $\Delta R(T=14)$ (panel (a)) and $RM(n+1)$ versus the 12-mma of $\Delta R(T=44)$ (panel (b)). Based on the known value ($= 1.9$) of cycle 23's $\Delta R(T=14)$, the RM for cycle 24 is estimated to be about 139 ± 67 (the 90-percent prediction interval); while, based on the known value ($= -1.88$) of cycle 23's 12-mma of $\Delta R(T=44)$, the RM of cycle 24 is estimated to be about 137 ± 69 .

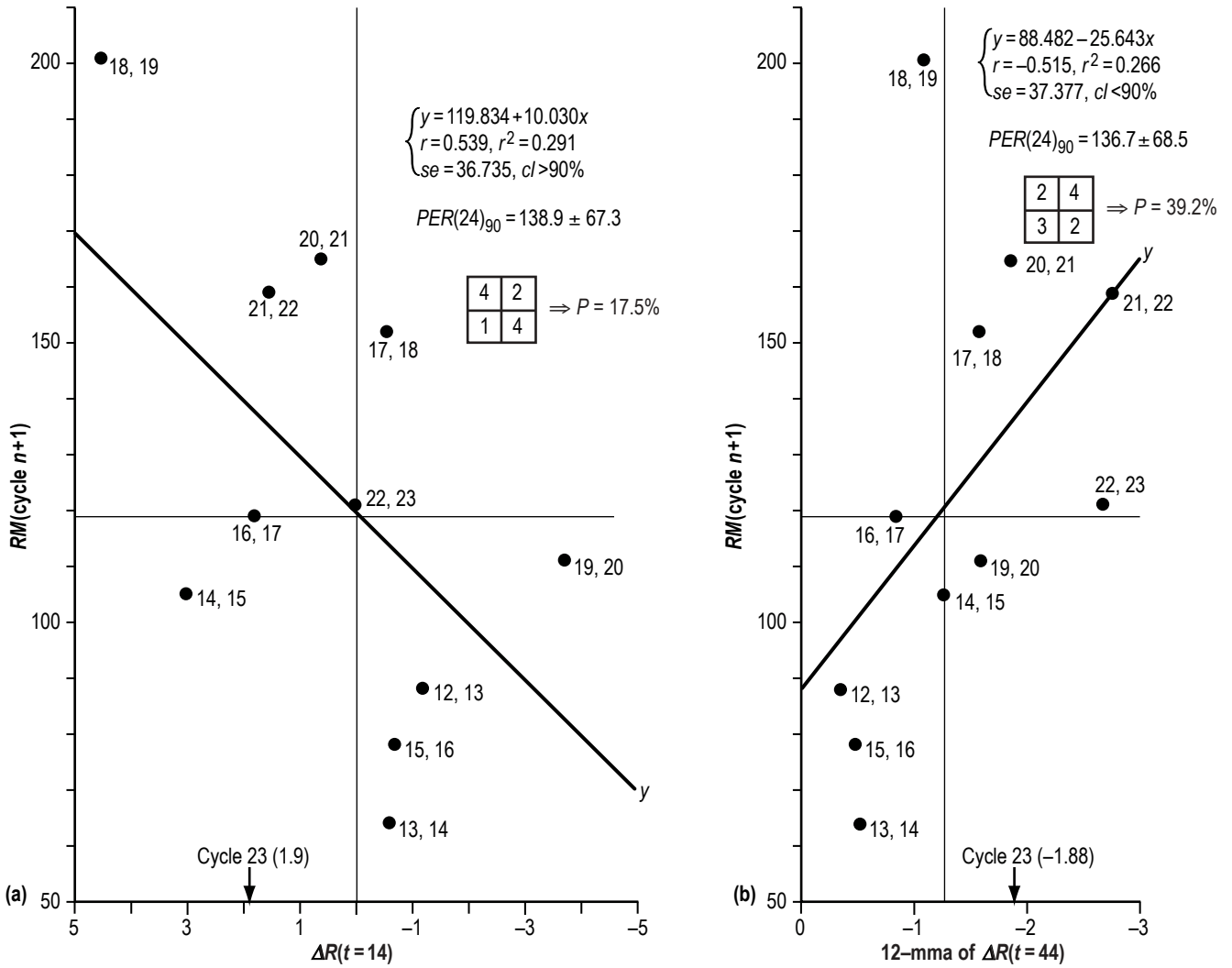


Figure 22. Scatter plots of $RM(\text{cycle } n+1)$ versus $\Delta R(T=14)$ and 12-mma of $\Delta R(T=44)$.

2.2.6 Slope_{ASC} and Slope_{DES}

Figure 23 displays the scatter plots of Slope_{ASC} (panel (c)) and Slope_{DES} (panel (a)) versus ΔR maxpos and Slope_{ASC} (panel (d)) and Slope_{DES} (panel (b)) versus (12-mma of ΔR)maxpos, where Slope_{ASC} is defined as $(RM - Rm)/ASC$ and Slope_{DES} is defined as $((Rm \text{ for cycle } n+1) - (RM \text{ for cycle } n))/DES$ for cycle n . All correlations are inferred to be highly statistically important, especially Slope_{DES} versus (12-mma of ΔR)maxpos. Estimates (90-percent prediction intervals) of Slope_{DES} for cycle 23 are made based on the observed values of ΔR maxpos and (12-mma of ΔR)maxpos.

Figure 24 shows scatter plots of Slope_{DES} versus ΔR maxneg (panel (a)), (12-mma of ΔR)maxneg (panel (b)), and Slope_{ASC} (panel (c)). Again, all correlations are inferred to be highly statistically important, especially Slope_{DES} versus Slope_{ASC}. Estimates (90-percent prediction intervals) of Slope_{DES} for cycle 23 are made based on the observed values of ΔR maxneg, (12-mma of ΔR)maxneg, and Slope_{ASC}.

Of the various estimates for Slope_{DES}, the best estimate (smallest 90-percent prediction interval) appears to be the one based on (12-mma of ΔR)maxpos. Hence, cycle 23's Slope_{DES} likely will measure about -1.15 ± 0.29 .

2.2.7 Cycle 23 Behavior: May 1996–August 2007

Figure 25 displays the 12-mma of R (panel (b)) for elapsed times $t=0$ (May 1996)–135 (August 2007). The 12-mma of ΔR for elapsed times $t=0$ (May 1996)–128 (January 2007) is also shown. For convenience, the values of Rm , RM , ASC , DES , PER , (12-mma of ΔR)maxpos, and (12-mma of ΔR)maxneg and the dates of occurrence of $E(Rm)$, $E(RM)$, $E((12\text{-mma of } \Delta R)\text{maxpos})$, and $E((12\text{-mma of } \Delta R)\text{maxneg})$ are given. Thus, RM for cycle 23 measured 120.8 (occurring at $t=47$, April 2000) and the value of R at $t=135$ mo (August 2007) measured 6.1. The current Slope_{DES} is $(6.1 - 120.8)/88 = -1.30$, which is within the window of the estimated value for cycle 23's Slope_{DES} ($= -1.15 \pm 0.29$), inferring that $E(Rm)$ for cycle 24 is imminent. Recall from figure 6 that the time ($t(4)$) from $E((12\text{-mma of } \Delta R)\text{maxneg})$ to $E(Rm)$ of the following cycle averages about 51 mo (with $sd=10$), inferring that $E(Rm)$ for cycle 24 should follow November 2002 ($t=78$) by about 51 ± 18 mo (the 90-percent prediction interval), or that there is a 95-percent P that cycle 24 will have its official onset before September 2008. (Since R is now known through September 2007, the actual Slope_{DES} is -1.29 .)

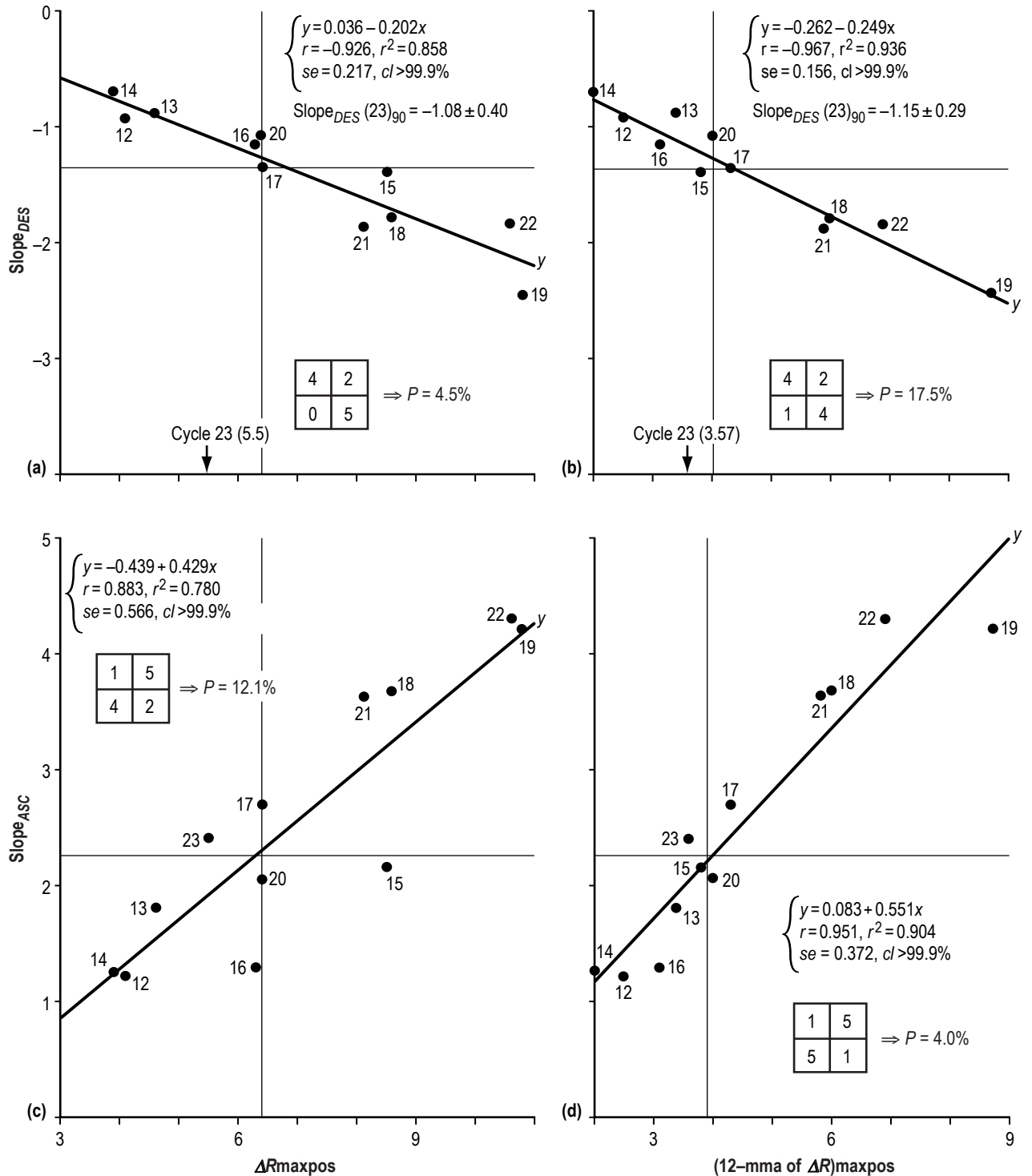


Figure 23. Scatter plots of Slope_{ASC} versus ΔR_{maxpos} and $(12-\text{mma of } \Delta R)_{\text{maxpos}}$ and of Slope_{DES} versus ΔR_{maxpos} and $(12-\text{mma of } \Delta R)_{\text{maxpos}}$.

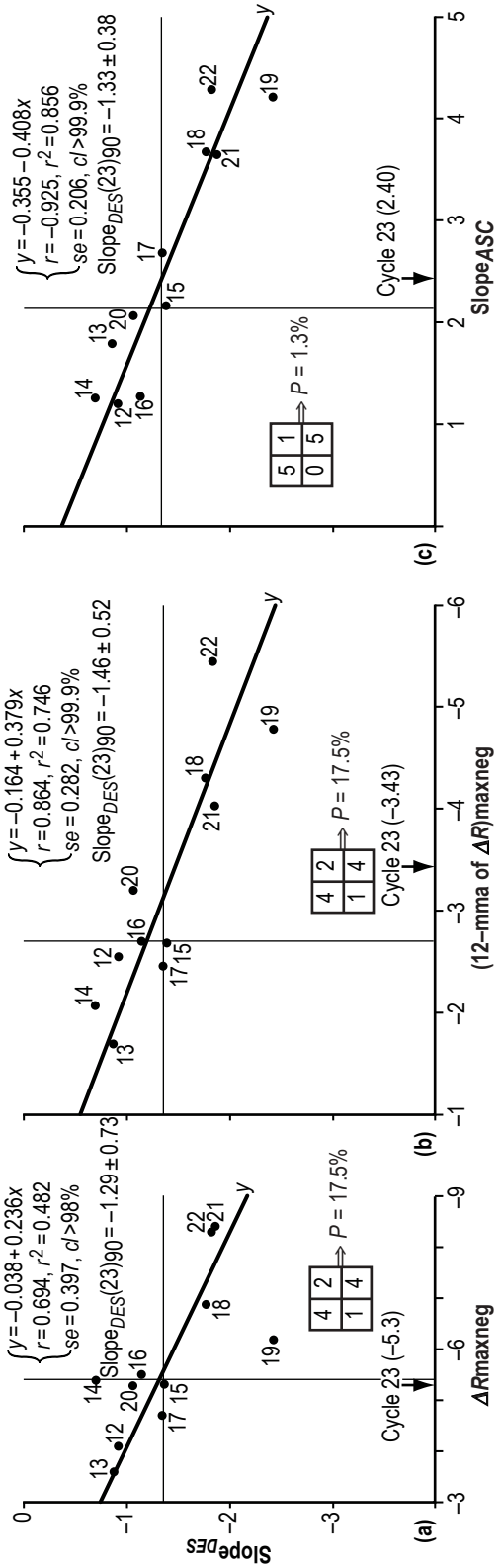


Figure 24. Scatter plots of Slope_{DES} versus ΔR maxpos, (12-mma of ΔR)maxpos, and Slope_{ASC}.

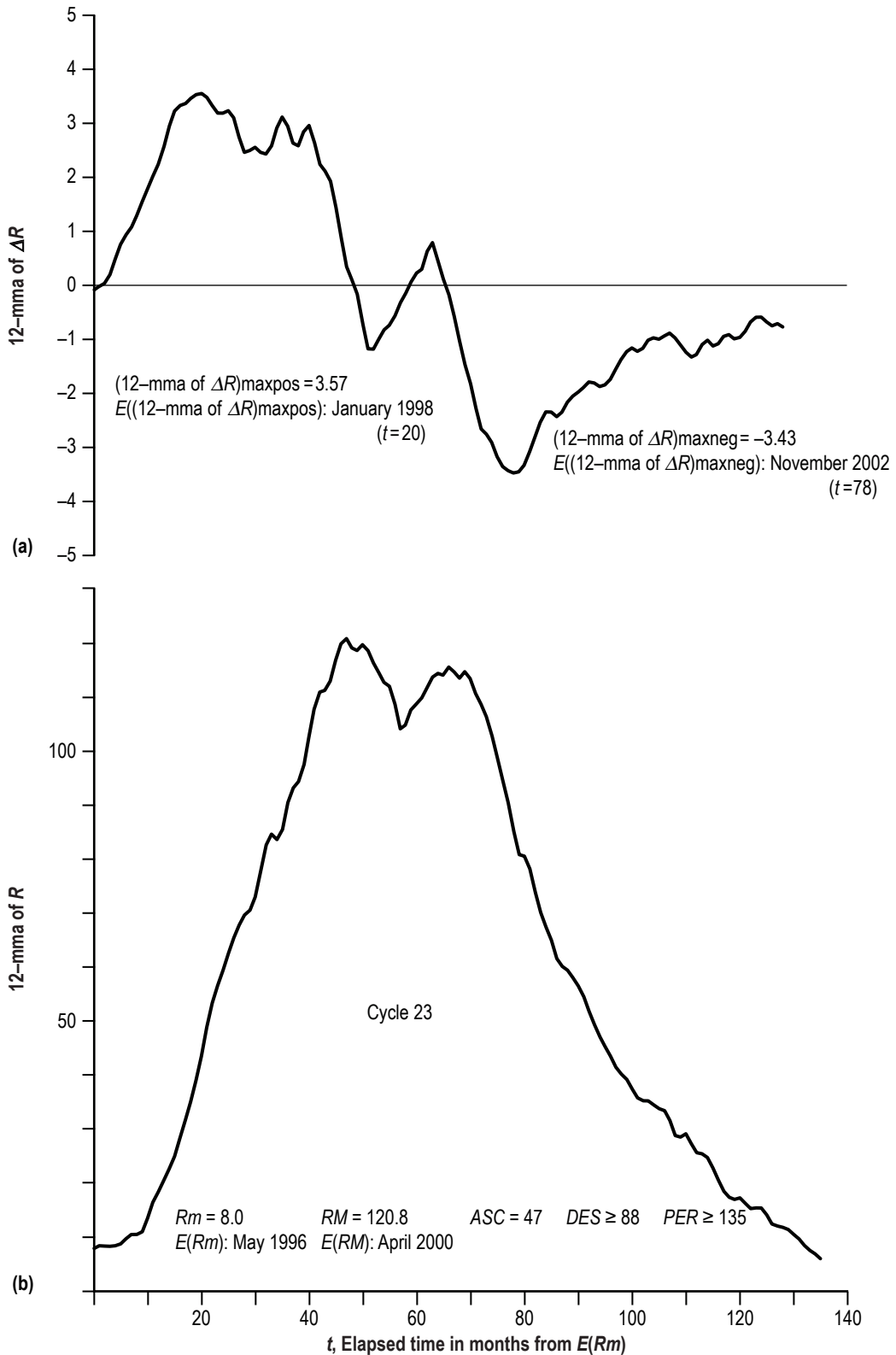


Figure 25. Variation of cycle 23's R and 12-mma of ΔR for $t = 0\text{--}135$ (May 1996–August 2007).

3. SUMMARY

Various methods,^{4,19–22} those using geomagnetic precursor information in particular, have been used to successfully predict RM several years in advance of its occurrence. For cycle 24, the next sunspot cycle, precursor techniques suggest that it will have an RM equal to about 130 ± 14 (see Wilson and Hathaway²² and references contained therein), peaking about 44 ± 5 mo after $E(Rm)$, or about November 2011 (± 5 mo) if the official start of cycle 24 is, indeed, March 2008, as predicted by the NOAA Solar Cycle 24 Prediction Panel.¹⁴ This prediction for the size of cycle 24's RM is more supportive of the higher consensus prediction of the NOAA panel (140 ± 20) than its lower consensus prediction (90 ± 10), where the two consensus predictions arise from consequences of two different dynamo-related techniques. So, it is with great anticipation²³ that solar researchers await the start and rise of cycle 24.

Once a cycle officially gets underway, predictions of the level of future activity based on autoregressive techniques^{24,25} and other curve-fitting methods^{6,9,19} can be employed. As found in this Technical Publication and in previous studies,^{2,6,7,9,19} the size (RM) of the cycle can be better predicted about 2 yr into the rise of a sunspot cycle, especially once its ascending inflection point has been clearly discerned.

In this Technical Publication, it has been noted that, on the basis of cycles 12–23 (the most reliably determined sunspot cycles), cycles can be loosely grouped into three groups based on RM or two groups based on cycle duration. Large-amplitude cycles (cycles 18, 19, 21, and 22) tend to have higher values of Rm , rise to RM more quickly (shorter ASC), and have shorter cycle duration (shorter PER) than either average-amplitude cycles (cycles 15, 17, 20, and 23) or small-amplitude cycles (cycles 12, 13, 14, and 16). Likewise, short-period cycles (cycles 15–19, 21, and 22) tend to rise more quickly to RM and to have higher values of Rm and RM than long-period cycles (cycles 12–14, 20, and 23). It is also noted that, over the course of cycles 12–23, there have been statistically important secular rises in Rm and RM and in the values of R at the ascending (more positive) and descending (more negative) inflection points. On the basis of the secular increases, estimates have been made for cycle 24; namely, its Rm should measure about 11.5 ± 4.5 , its RM about 167 ± 64 , its ASC about 39 ± 11 mo, the value of its ΔR_{maxpos} about 9.4 ± 3.7 , the value of its ΔR_{maxneg} about -7.6 ± 2.0 , the value of its 12-mma ΔR_{maxpos} about 6.55 ± 3.03 , and the value of its 12-mma ΔR_{maxneg} about -4.83 ± 1.43 . Its PER will measure about 125 ± 18 mo.

This study has shown that the later occurring RM can be continually estimated by monitoring the month-to-month rate of change in R . For values of $\Delta R_{\text{maxpos}} \leq 6.4$, it is expected that $RM \leq 121$, while for values of $\Delta R_{\text{maxpos}} > 6.4$ it is expected that $RM > 105$. Based on the slope determined at ΔR_{maxpos} , RM can be predicted with even higher precision ($se = 10.6$). It was found that, as early as 10 mo after $E(Rm)$, the value of $\Delta R(t)$ can be used to estimate the later occurring RM , although the best result is determined about 2 yr into the cycle. Use of the 12-mma of ΔR to predict RM provides similar accuracy as compared to using the slope at ΔR_{maxpos} . Values of the (12-mma of ΔR) $\text{maxpos} \leq 4.25$ strongly suggest $RM \leq 121$, while higher values suggest a larger RM .

Both ΔR_{maxneg} and its 12-mma value appear to correlate with PER , such that cycle 23's PER is expected to persist no longer than 143 mo, inferring that cycle 24 should have its official start no later than May 2008. An examination of ΔR and its 12-mma value relative to $E(RM)$ suggests that Rm for cycle 24 will measure about 7.6 ± 4.4 . R measured 5.9 in September 2007, so Rm for cycle 24 is expected very soon. The (12-mma of ΔR) maxpos suggests that the Slope_{DES} for cycle 23 will measure about -1.15 ± 0.29 . The computed current Slope_{DES} for cycle 23 is -1.29 through September 2007 and is shrinking with the passage of time. On average, the length of time in months from (12-mma of ΔR) maxneg to Rm is 51 ± 18 mo (the 90-percent prediction interval). Thus, there is only a 5-percent chance that $E(Rm)$ for cycle 24 will occur after August 2008.

REFERENCES

1. Sunspot Index Data Center Web, <<http://sidc.oma.be/index.php3>> Accessed 2008.
2. Wilson, R.M.: “A Comparative Look at Sunspot Cycles,” *NASA TP 2325*, Marshall Space Flight Center, Alabama, May 1984.
3. Wilson, R.M.: “Predicting the Maximum Amplitude for the Sunspot Cycle From the Rate of Rise in Sunspot Number,” *Solar Phys.*, Vol. 117, pp. 179–186, 1988.
4. Wilson, R.M.: “On the Level of Skill in Predicting Maximum Sunspot Number: A Comparative Study of Single Variate and Bivariate Precursor Techniques,” *Solar Phys.*, Vol. 125, pp. 143–155, 1990.
5. Wilson, R.M.: “On the Maximum Rate of Change in Sunspot Number Growth and the Size of the Sunspot Cycle,” *Solar Phys.*, Vol. 127, pp. 199–205, 1990.
6. Hathaway, D.H.; Wilson, R.M.; and Reichmann, E.J.: “The Shape of the Sunspot Cycle,” *Solar Phys.*, Vol. 151, pp. 177–190, 1994.
7. Lantos, P.: “Prediction of the Maximum Amplitude of Solar Cycles Using the Ascending Inflexion Point,” *Solar Phys.*, Vol. 196, pp. 221–225, 2000.
8. Wilson, R.M.; and Hathaway, D.H.: “Gauging the Nearness and Size of Cycle Maximum,” *NASA/TP-003-212927*, Marshall Space Flight Center, Alabama <<http://trs.nis.nasa.gov/archive/00000650/>>, November 2003.
9. Wilson, R.M.; and Hathaway, D.H.: “Application of the Maximum Amplitude-Early Rise Correlation to Cycle 23,” *NASA/TP-2004-213281*, Marshall Space Flight Center, Alabama, <<http://trs.nis.nasa.gov/archive/00000674/>>, June 2004.
10. Wilson, R.M.; and Hathaway, D.H.: “An Examination of Sunspot Number Rates of Growth and Decay in Relation to the Sunspot Cycle,” *NASA/TP-2006-214433*, Marshall Space Flight Center, Alabama, <<http://trs.nis.nasa.gov/archive/00000731/>>, June 2006.
11. Hoyt, D.V.; and Schatten, K.H.: “Group Sunspot Numbers: A New Solar Activity Reconstruction,” *Solar Phys.*, Vol. 181, pp. 491–512, 1998.
12. Wilson, R.M.: “A Comparison of Wolf’s Reconstructed Record of Annual Sunspot Number With Schwabe’s Observed Record of ‘Clusters of Spots’ for the Interval of 1826–1868,” *Solar Phys.*, Vol. 182, pp. 217–230, 1998.

13. Waldmeier, M.: *The Sunspot-Activity in the Years 1610–1960*, Schulthess & Co., Zurich, Switzerland, 1961.
14. Space Weather Prediction Center Web, <<http://www.swpc.noaa.gov/SolarCycle/SC24/index.html>> Accessed 2008.
15. Wilson, R.M.; Hathaway, D.H.; and Reichmann, E.J.: “On the Importance of Cycle Minimum in Sunspot Cycle Prediction,” *NASA TP-3648*, Marshall Space Flight Center, Alabama, <<http://trs.nis.nasa.gov/archive/00000335/>>, August 1996.
16. Wilson, R.M.: “On the Long-Term Secular Increase in Sunspot Number,” *Solar Phys.*, Vol. 115, pp. 397–408, 1988.
17. Hathaway, D.H.; Wilson, R.M.; and Reichmann, E.J.: “Group Sunspot Numbers: Sunspot Cycle Characteristics,” *Solar Phys.*, Vol. 211, pp. 357–370, 2002.
18. Evert, B.S.: *The Analysis of Contingency Tables*, John Wiley & Sons Inc., New York, New York, p. 15, 1977.
19. Hathaway, D.H.; Wilson, R.M.; and Reichmann, E.J.: “A Survey and Synthesis of Solar Cycle Prediction Techniques,” *J. Geophys. Res.*, Vol. 104, pp. 22,375–22,388, 1999.
20. Hathaway, D.H.; and Wilson, R.M.: “Geomagnetic Activity Indicates Large Amplitude for Sunspot Cycle 24,” *Geophys Res. Lett.*, 33, p. L18,101, doi:10.1029/2006GL027053, 2006.
21. Wilson, R.M.; and Hathaway, D.H.: “An Examination of Selected Geomagnetic Indices in Relation to the Sunspot Cycle,” *NASA/TP-2006-214711*, Marshall Space Flight Center, Alabama, <<http://trs.nis.nasa.gov/archive/00000741/>>, December 2006.
22. Wilson, R.M.; and Hathaway, D.H.: “Using the Modified Precursor Method to Estimate the Size of Cycle 24,” *NASA/TP-2008-215467*, Marshall Space Flight Center, Alabama, July 2008.
23. Wilson, R.M.; and Hathaway, D.H.: “Anticipating Cycle 24 Minimum and Its Consequences,” *NASA/TP-2007-215134*, Marshall Space Flight Center, <<http://trs.nis.nasa.gov/archive/00000768/>>, November 2007.
24. McNish, A.G.; and Lincoln, J.V.: “Prediction of Sunspot Numbers,” *Eos Trans. AGU*, Vol. 30, pp. 673–685, 1949.
25. Greer, M.S.: “New Procedures for SESC Sunspot Number and 10.7-cm Flux Prediction,” in *IV: Proceedings of a Workshop at Ottawa, Canada*, J. Hruska, M.A. Smart, D.F. Smart, and G. Hechman (eds.), National Oceanic and Atmospheric Administration, Environmental Research Laboratory, Boulder, Colorado, Vol. 2, pp. 172–179, 1993.

REPORT DOCUMENTATION PAGE			Form Approved OMB No. 0704-0188
<p>Public reporting burden for this collection of information is estimated to average 1 hour per response, including the time for reviewing instructions, searching existing data sources, gathering and maintaining the data needed, and completing and reviewing the collection of information. Send comments regarding this burden estimate or any other aspect of this collection of information, including suggestions for reducing this burden, to Washington Headquarters Services, Directorate for Information Operation and Reports, 1215 Jefferson Davis Highway, Suite 1204, Arlington, VA 22202-4302, and to the Office of Management and Budget, Paperwork Reduction Project (0704-0188), Washington, DC 20503</p>			
1. AGENCY USE ONLY (Leave Blank)	2. REPORT DATE	3. REPORT TYPE AND DATES COVERED	
	September 2008	Technical Publication	
4. TITLE AND SUBTITLE	Using the Inflection Points and Rates of Growth and Decay to Predict Levels of Solar Activity		5. FUNDING NUMBERS
6. AUTHORS	Robert M. Wilson and David H. Hathaway		
7. PERFORMING ORGANIZATION NAME(S) AND ADDRESS(ES)			8. PERFORMING ORGANIZATION REPORT NUMBER
George C. Marshall Space Flight Center Marshall Space Flight Center, AL 35812		M-1240	
9. SPONSORING/MONITORING AGENCY NAME(S) AND ADDRESS(ES)			10. SPONSORING/MONITORING AGENCY REPORT NUMBER
National Aeronautics and Space Administration Washington, DC 20546-0001		NASA/TP—2008-215473	
11. SUPPLEMENTARY NOTES Prepared for the Science and Exploration Vehicle Office, Science and Mission Systems Office			
12a. DISTRIBUTION/AVAILABILITY STATEMENT Unclassified-Unlimited Subject Category 92 Availability: NASA CASI 301-621-0390		12b. DISTRIBUTION CODE	
13. ABSTRACT (Maximum 200 words) The ascending and descending inflection points and rates of growth and decay at specific times during the sunspot cycle are examined as predictors for future activity. On average, the ascending inflection point occurs about 1–2 yr after sunspot minimum amplitude (R_m) and the descending inflection point occurs about 6–7 yr after R_m . The ascending inflection point and the inferred slope (including the 12-mo moving average (12-mma) of ΔR (the month-to-month change in the smoothed monthly mean sunspot number (R)) at the ascending inflection point provide strong indications as to the expected size of the ongoing cycle's sunspot maximum amplitude (RM), while the descending inflection point appears to provide an indication as to the expected length of the ongoing cycle. The value of the 12-mma of ΔR at elapsed time $T = 27$ mo past the epoch of RM ($E(RM)$) seems to provide a strong indication as to the expected size of Rm for the following cycle. The expected Rm for cycle 24 is 7.6 ± 4.4 (the 90-percent prediction interval), occurring before September 2008. Evidence is also presented for secular rises in selected cycle-related parameters and for preferential grouping of sunspot cycles by amplitude and/or period.			
14. SUBJECT TERMS Sun, sunspot cycle, solar activity, sunspot cycle prediction, inflection points, sunspot growth rates		15. NUMBER OF PAGES 48	16. PRICE CODE
17. SECURITY CLASSIFICATION OF REPORT Unclassified	18. SECURITY CLASSIFICATION OF THIS PAGE Unclassified	19. SECURITY CLASSIFICATION OF ABSTRACT Unclassified	20. LIMITATION OF ABSTRACT Unlimited

National Aeronautics and

Space Administration

IS20

George C. Marshall Space Flight Center

Marshall Space Flight Center, Alabama

35812